Australian Government
Department of Defence
Defence Science and
Technology Organisation

Turbulent Dispersion Modelling in a Complex Urban Environment – Data Analysis and Model Development

Alexei T. Skvortsov, Peter D. Dawson, Michael D. Roberts and Ralph M. Gailis

Human Protection and Performance Division

Defence Science and Technology Organisation

DSTO–TR–2366

ABSTRACT

This report summarises recent research conducted by the DSTO in plume model development for urban environments, with an emphasis on establishing clear physical grounds for the models, yet maintaining enough simplicity to be treated numerically in an operationally viable way. The aim is not to replace existing operational models with a new generation of more accurate models, but to provide a more physics-based framework for flow and dispersion in an urban environment that can reconcile the empirically based approach of current operational models, and the more sophisticated computational fluid dynamics techniques now gaining popularity for atmospheric dispersion applications. A key feature of the model framework developed in this report is the definition of a single parameter that describes canopy morphology, and links this to canopy flow variables. A simple canopy dispersion model is then developed, based on flow parameters generated by the canopy model. In relevant areas the well-known Urban Dispersion Model by the UK Defence Science and Technology Laboratory is used as a benchmark for comparison. Supporting evidence for the models developed here is supplied through comparison with experimental data from a water channel simulation.

Published by

DSTO Defence Science and Technology Organisation
506 Lorimer St,
Fishermans Bend, Victoria 3207, Australia

Telephone: (03) 9626 7000
Facsimile: (03) 9626 7999

AR No. AR–014–674
February, 2010

APPROVED FOR PUBLIC RELEASE

Turbulent Dispersion Modelling in a Complex Urban Environment – Data Analysis and Model Development

Executive Summary

The purpose of this report is to summarise the recent research conducted by the Defence Science and Technology Organisation (DSTO) in the development of a modelling framework for predicting the dispersion of chemical, biological or radiological (CBR) contaminants in urban environments. In relevant areas the well-known empirically based Urban Dispersion Model (UDM) developed by the UK Defence Science and Technology Laboratory (Dstl) is used as a benchmark for comparison. Comparisons are also made with some more practically oriented computational fluid dynamics (CFD) models that are receiving considerable interest in the literature.

The aim is not to replace existing operational models with a new generation of more accurate models—the broad scope of issues and problems to be addressed in completing such a task is not able to be attempted here, and the enhancement of operational capability from such an undertaking is far from clear. Rather, we provide a more physics-based framework for flow and dispersion models in an urban environment that can to some extent reconcile the very empirically based approach of models such as the UDM, and the more sophisticated CFD models. In developing such a framework, we are able to better interpret experimental data for validation of various models, and provide a starting point for the development of more complex concentration fluctuation models. Such models are a challenge to formulate in an urban environment, but ultimately are required for the development of synthetic CBR environments to predict realistic fluctuating challenge levels, toxicity response, optimal detector networks, data fusion algorithms for enhanced CBR situational awareness, and the rigorous quantification of uncertainty in dispersion predictions.

To achieve clarity in the range of approaches available for practical models of contaminant dispersion in urban areas, an overview of various methods recently developed for turbulent transport and mixing over an inhomogeneous canopy is presented in Section 2. The analytical complexity of those methods is simplified to a degree that allows straightforward practical implementation and application.

Using these results as a foundation, in Section 3 a new theoretical framework is proposed based on matching flow parameters inside and outside the canopy. The proposed theoretical framework can help to validate and justify some heuristic assumptions of the UDM and may be used as a valuable performance check in other dispersion models. A key feature of this model framework is the definition of a single parameter that describes canopy morphology, and links this to canopy flow variables. The flow model is used as input to a dispersion model for the canopy.

In Section 4 the theoretical findings are validated against experimental data collected from water channel simulations of dispersion through a variety of different obstacle arrays. These arrays provide a systematic approach to investigating the effects of differing obstacle morphology on flow and dispersion. The degree to which the model can reproduce various plume effects due to the canopy morphology is discussed.

The framework developed allows a link between previously published DSTO work on

fluctuating plume models in urban settings [30, 33], current DSTO–Commonwealth Scientific and Industrial Research Organisation (CSIRO) collaborative work on internal concentration fluctuations [37], and more complex distributed drag CFD models in urban areas [18, 19, 20]. This will enable a high fidelity model of urban dispersion to be implemented for emergency response applications, with the extra capability for predicting concentration fluctuations. A pilot system involving coupling between a nested hierarchy of mesoscale meteorological models, CFD models and Lagrangian particle models has already been established by Environment Canada in collaboration with Defence Research & Development Canada (DRDC) and various Canadian universities [2, 3]. The methodology developed here serves as an interim step, contributing to extra capability for concentration fluctuation prediction and characterisation of the uncertainty in modelling predictions. There is also potential for a similar system to be implemented within Australia.

The framework developed has also provided a link through the UDM to another important operational modelling capability that DSTO now possesses—the CBR Virtual Battle-space developed by Dstl. There is further scope for development of concentration realisation models within this capability framework. Finally, the generation of prototype simple synthetic environments for plume realisations is also required to further develop data fusion algorithms for CBR source characterisation and network detection. The framework developed here is the first step in the development of such a synthetic environment here at DSTO for these purposes, and can ultimately be used to compare the approaches studied at DSTO with those of our international collaborators.

Contents

Appendices

Figures

Glossary

[ABL] Atmospheric Boundary Layer

[CBR] Chemical, Biological and Radiological

[CFD] Computational Fluid Dynamics

[CSIRO] Commonwealth Scientific and Industrial Research Organisation

[DNS] Direct Numerical Simulation

[DRDC] Defence Research and Development Canada

[Dstl] Defence Science and Technology Laboratory, UK

[NS] Navier Stokes

[UDM] Urban Dispersion Model

1 Introduction

There exists a large variety of approaches in attempting to solve the difficult problem of atmospheric dispersion modelling in urban environments. Predicting the evolution of a plume is a complex problem, to be described by advanced methods of fluid dynamics, the theory of turbulence and diffusion, and statistics. Its comprehensive modelling is computationally very intensive and time consuming. However in an operational environment, a prediction is needed quickly.

The UK Defence Science and Technology Laboratory (Dstl) Urban Dispersion Model (UDM) [1] provides an example of an effective operational model that can provide quick answers to threat scenarios of the release of chemical, biological or radiological (CBR) material of gas or aerosol form into an urban environment. Understandably, such quick running models are based on many heuristic and practical assumptions, and rely heavily on empirical parameters derived under certain experimental conditions that are not always clearly extendable to a wider variety of atmospheric conditions.

On the other hand, there has been growing interest in the use of computational fluid dynamics models (CFD) for modelling contaminant dispersion in urban areas. Although more physically based, these models tend to be computationally intensive, and require considerably greater computational resources (in both computing power and time), so that they are not generally practical for operational situations. Despite the greater emphasis on the underlying physics in these models, the inherent complexity of flow in real urban environments, and the many approximations and empiricism still required in the formulation of these models does not necessarily imply that they provide significantly more accurate predictions.

This report summarises recent work at DSTO in developing a modelling framework to describe the dispersion of CBR contaminants in an atmospheric boundary layer (ABL) over a heterogeneous surface. The aim is not to replace existing operational models with a new generation of more accurate models—the broad scope of issues and problems to be addressed in completing such a task is not able to be attempted here, and the enhancement of operational capability from such an undertaking is far from clear. Rather, we provide a more physics-based framework for flow and dispersion models in an urban environment that can reconcile to some extent the very empirically based approach of models such as the UDM, and the more sophisticated CFD models (being developed for example for Canadian civilian emergency response capability [2, 3]). In developing such a framework, we are able to better interpret experimental data for validation of various models, and provide a starting point for the development of more complex concentration fluctuation models. Such models are a challenge to formulate in an urban environment, but ultimately are required for the development of synthetic CBR environments to predict realistic fluctuating challenge levels. Concentration fluctuations are important in analysing toxicity response, optimal detector networks, data fusion algorithms for enhanced CBR situational awareness, and the rigorous quantification of uncertainty in dispersion predictions.

In order to give a background understanding of previous work in this area, in Section 2 a brief overview of the complex modelling methods recently developed for turbulent transport and mixing is presented. In Section 3 a new theoretical framework is proposed based on matching flow parameters inside and outside the canopy. The proposed theoretical

framework can help to validate and justify some heuristic assumptions of the UDM, and may be used as a valuable performance check in other dispersion models. In Section 4 data from our water channel experimental data are used in validating our theoretical findings.

2 An Overview of Turbulent Dispersion in the Urban Boundary Layer

2.1 Velocity Field in the Urban Boundary Layer

Since flow in the ABL is a key driver for CBR pollutant advection and dispersion, the development of a high fidelity model of this flow is a crucial step in the modelling of the whole turbulent dispersion process.

The simplest model of flow in the ABL is the celebrated log-law profile [4]. With coordinate x the downstream distance from the source, y is the crosswind coordinate, and $z \geq 0$ the height above the ground, the vertical profile of mean flow aligned with the x-axis takes the form

$$U(z) = \frac{u_*}{\kappa} \log\left(\frac{z}{z_0}\right), \tag{1}$$

where u_* is the friction velocity, $\kappa = 0.41$ is von Karman's constant, $z_0 = \nu/u_*$ is the viscous length[1], and ν is the viscosity. Equation (1) is valid in the surface layer portion of the ABL, for neutral stability conditions.

It has been known for a long time (dating back to Prandtl [4]) that the ABL velocity profile can be fairly approximated by a power-law function:

$$U(z) = a u_* \left(\frac{z}{z_0}\right)^m, \tag{2}$$

where a and m are constants. This profile, being algebraically simpler than the log-law profile, has been used merely as a convenient engineering approximation, but recently it has attracted much attention after being shown that it can be justified based on a self-similarity property of the ABL flow. For the boundary layer over a flat smooth surface, it was rigorously shown by Barenblatt *et al* [5, 6] that

$$a = \frac{\log Re}{\sqrt{3}} + \frac{5}{2}, \quad m = \frac{3}{2\,\ln Re}, \tag{3}$$

where Re is the Reynolds number of the flow. For our purposes we assume that both profiles (1) and (2) hold equally for turbulent flow in the ABL with parameters a and m to be determined from data fitting. This is justified due to the stochastic nature of atmospheric flows. The flow variables in the atmosphere do not remain statistically stationary for long enough for truly converged mean quantities, so the resulting uncertainty in measured profiles of mean velocity usually cannot provide a distinction between (1) and (2).

[1] for flow over smooth surfaces, or roughness length for flow over rough surfaces

Observed values of m in the atmosphere range from nearly 0 in very unstable conditions, representing perfect mixing and a uniform velocity profile, to nearly 1 in very stable conditions, approaching the Couette linear profile of laminar motion over a plane surface. In neutral conditions $m \approx 1/7$ [4] (a thorough discussion of wind profiles in different weather conditions can be found in [35]). The value of m also depends on surface roughness: roughness promotes mixing near the surface, which reduces the velocity gradient at small z and thus leads to larger m. These effects can be computed in a semi-empirical way and the UDM [1] also provides a framework for this. While it is acknowledged that the two profile forms are not mathematically equivalent, we use both forms in various parts of this report to derive tractable analytical models of flow and dispersion within urban areas that would not be possible by restricting ourselves to just one choice.

The turbulent (or eddy) viscosity in the ABL can be determined as

$$K(z) = K_0 \left(\frac{z}{z_0}\right)^n. \tag{4}$$

where K_0 and r are constants. The value of n can be specified based on various analytical models of turbulent boundary layers or directly estimated from the observational data. In particular, for so-called conjugate power-law profiles (constant momentum flux) [4]

$$n = 1 - m, \tag{5}$$

and for Monin-Obukhov similarity profiles

$$n = 1. \tag{6}$$

In general, we may still consider n as a free independent parameter of the flow model.

Over a rough surface (i.e. ABL over canopy) the profiles (1) and (2) are modified according to

$$U(z) = \frac{u_*}{\kappa} \log\left(\frac{z-d}{z_0}\right), \tag{7}$$

$$U(z) = a u_* \left(\frac{z-d}{z_0}\right)^m, \tag{8}$$

where now z_0 is the roughness height and d is the so-called displacement height. Both d and z_0 should be considered as new fitting parameters of the ABL flow over the canopy, and their simple physical interpretation is not always obvious. For instance (7) still produces meaningful results even for $d < 0$, when its naive interpretation as the "ABL flow displacement by canopy" is not feasible. It is worth pointing out that determining z_0 and d simultaneously from experimental data is problematic. The difficulty arises from the log relationship, which causes an exponential dependency of the parameters on uncertainties in the measured data. This problem has been described in more detail by Gailis [7], and demonstrated rigorously in a Bayesian inference framework for certain data-sets [8].

The ongoing challenge for any plausible model of ABL flow over the heterogeneous canopy is to establish reliable functional relationships between z_0, d and the parameters of the canopy (i.e. building morphology). Once such relationships are found, they can be used in conjunction with (7) or (8) to model the mean velocity profile affected by a

particular canopy. Such a modified velocity profile can later be used as an input for the pollutant transport equation (21).

Various simple approaches based on empirical relations can be found in the literature to relate canopy parameters to velocity profile parameters. These approaches tend to use formulas with some physical basis, but often coupled with heuristic assumptions and heavily reliant on tuning the relationships to specific data. Two older examples include those of Lettau [9] and Counihan [10]. The approach used in the UDM [1] was developed by Macdonald *et al* [11], and attempts to base the relationships on firmer physical grounds. The first key canopy parameter is the ratio of the collective frontal area of the obstacles to the collective horizontal area of the canopy (called the lot area):

$$\lambda_f = \frac{A_f}{A_d}, \tag{9}$$

i.e. the density of the windward faces of the canopy (which is equivalent to leaf area density for plant canopies). The second key canopy parameter is the ratio of the summed horizontal area of objects in the canopy (plan area) to the lot area

$$\lambda_p = \frac{A_p}{A_d}, \tag{10}$$

or the dimensionless plan area. Then, given the averaged canopy height H, and the drag coefficient C_D of individual canopy elements, some simple considerations of shear stress give the following relationships [11]:

$$\frac{d}{H} = 1 + A^{-\lambda_p}(\lambda_p - 1), \tag{11}$$

$$\frac{z_0}{H} = \left(1 - \frac{d}{H}\right) \exp\left\{-\left[\frac{\beta}{2}\frac{C_D}{\kappa^2}\left(1 - \frac{d}{H}\right)\lambda_f\right]^{-1/2}\right\}. \tag{12}$$

Here $\kappa = 0.41$ is von Karman's constant, and we have two constants A and β that are tunable according to particular obstacle arrays. For a regular cubic array, $A = 3.59$ and $\beta = 0.55$, whereas for a staggered cubic array, $A = 4.43$ and $\beta = 1.0$. We observe that $d = 0$ and $z_0 = 0$ for $\lambda_p = 0$ (no canopy), and $d = H$ and $z_0 = 0$ for $\lambda_p = 1$ (full packing).

The formulae (8), (11) and (12) are the core components of the surface layer flow model in the UDM and plots for d and z_0 corresponding to these formulae are presented in Figure 25 of the technical documentation [1]. In Section 3.1 we will provide a theoretical framework in order to derive some analytical relationships between z_0, d and the parameters of the canopy. This will help to validate and justify some of the heuristic assumptions and tuning used to generate the relationships (11) and (12) as employed in the UDM, and may be used as a valuable performance check in other dispersion models.

The approach outlined above is simple and uses some physics-based arguments, but is primarily given its predictive power through empirical relationships. More advanced approaches rely on utilising the full fluid dynamics equations of the canopy flows—usually referred to as the Navier Stokes (NS) equations—with various simplifying approximations and empirical inputs. The entire range of techniques in computational fluid dynamics (CFD) is very broad and beyond the scope of this report, but here we focus on one approach that has already been demonstrated as useful for practical applications involving

relatively stringent time and computational requirements. This more advanced approach to surface layer flow in the canopy is to compute the mean flow by solving the time and space averaged momentum equations. Thus influence of the canopy is taken into account in a bulk fashion (as opposed to detailed point by point modelling) through its viscous drag and form (pressure difference) drag on the flow, which consequently has led to the name "distributed drag" for this class of models.

Relatively straightforward implementations of the distributed drag approach, including a systematic description of various flow regions/features in a canopy, and physical approximations that may be made within these regions have been given by Belcher *et al* [13] and Coceal *et al* [14, 15]. A more complex approach is to implement a modified spatially averaged k-ϵ CFD model, which includes budget equations for the turbulent kinetic energy k and turbulent dissipation ϵ, as demonstrated by Katul *et al* [16]. The above mentioned studies have all made some implicit assumptions in the derivation of the spatially and Reynolds averaged[2] NS equations, most importantly a neglect of the dispersive stresses[3] arising from the spatial averaging operation. Lien *et al* [18, 19] put the mathematical framework in dealing with time and spatial averaging of NS and k-ϵ equations on a rigorous footing, and demonstrated the non-commutation of the spatial and time averaging operators, which led to different structural equations ultimately describing the same physics, depending on whether spatial or time averaging is applied first. By comparing results with high resolution Reynolds-averaged k-ϵ NS models, they also demonstrated that the dispersive stresses were at times of great importance in canopies with urban morphology[4] [20].

For the purposes of this report, it is sufficient to take the following form for the mean momentum equations, without elaborating on the mathematical details for the issues raised in the previous paragraph:

$$\frac{\partial v_i}{\partial t} + v_j \frac{\partial v_i}{\partial x_j} = -\frac{\partial p}{\partial x_i} - \frac{\partial T_{ij}}{\partial x_j} - f_i, \quad f_i = \frac{|\mathbf{v}| v_i}{L_c}, \tag{13}$$

where T_{ij} is a spatially-averaged Reynolds stress, and f_i is a smoothly-varying canopy element drag (which arises from spatially averaging the localised drag due to individual roughness elements). The parameter

$$L_c = \frac{2H}{C_D(z)} \frac{(1-\lambda_p)}{\lambda_f} \tag{14}$$

does not depend on velocity and is called the canopy drag length scale; as before, H is the average height of canopy objects, and λ_f and λ_p are morphological parameters of the canopy. The physical meaning of L_c is a length-scale for an incident wind profile to adjust to the canopy (for typical values of L_c, see [13]).

[2]Reynolds averaging is ensemble- averaging and reduces to time averaging for statistically stationary flows.

[3]Specifically, the dispersive stresses arise from the spatial correlation in the time-mean velocity field as it varies with position in an averaging volume.

[4]Other studies of urban canopies have asserted that dispersive stresses are negligible by quoting data in the literature taken from plant canopies. Although this may be correct for plant canopies, it will be demonstrated below (and similarly has been stated in the urban canopy literature) that morphological parameters are considerably different between urban and plant canopies, so that conclusions drawn from plant canopy data are not necessarily transferable.

The formula (14) often permits further simplification by specifying height-averaged $\overline{C}_D$.[5] For the flow over a canopy consisting of a cubical array $\overline{C}_D \approx 2$ [13] ($\overline{C}_D \approx 1.2$ in the UDM [1][6]), so (14) can be reduced to

$$\epsilon = H/L_c \approx \frac{\lambda_f}{(1-\lambda_p)}, \tag{15}$$

where we introduced the non-dimensional "canopy density" parameter ϵ for convenience. Since ϵ is the only parameter determined by the canopy in the "distributed drag" framework, it is the parameter that should be used for any canopy parameterisation.[7] In Section 3 we will analytically derive expressions for d and z_0 via ϵ.

It is evident that canopies with higher ϵ are denser (for example, the case of $\lambda_p = 1$ corresponds to $\epsilon = \infty$ i.e. when the whole underlying surface is occupied by the canopy). In general $\epsilon \sim 1$ for urban canopies and $\epsilon \gg 1$ for plant canopies. In sparse canopies, horizontal momentum flux from the ABL flow is not influenced much by the canopy, and it directly applies to the underlying surface; otherwise in dense canopies all drag is fully absorbed by the canopy elements. In some respects a sparse canopy case is more challenging since it requires imposing the correct boundary condition for mean velocity $U(z)$ on the underlying surface. This depends of the fraction of drag propagating down to the surface and is not known beforehand (in dense canopies we simply have $\mathrm{d}U(z)/\mathrm{d}z = 0$ at $z = 0$).

To illustrate the significance of the canopy parameters described in this framework with a simple example, we consider a canopy consisting of a regular array of identical cylinders with radius r_0 and height H, separated by a distance of $2r_0$.[8] In this example, the expression (15) undergoes further simplification, with $\lambda_f = (2H/\pi r_0)\lambda_p$, and $C_D \approx 1$, so the formula can be reduced to

$$\epsilon \approx \frac{H}{2\pi r_0}\frac{\lambda_p}{1-\lambda_p}. \tag{16}$$

We can see how the value of parameter ϵ depends on the contribution of two factors: the shape of individual elements of the canopy and their packing density. None of these parameters separately determines the limiting value of ϵ in the case $\lambda_p \to 1$ or $H \to 0$, $r_0 \to 0$. In Sections 3.1 and Appendix A we argue that the limit should be taken in conjunction with $H \to 0$. Of course, this formula can be used for approximate estimation of ϵ for a canopy consisting of other elements, not just cylinders.

In order to derive any analytical solution of (13), a closure assumption must be used. The spatially-averaged Reynolds stress is usually represented with eddy viscosity models

[5] This is particularly important in plant canopies, where considerably different drag is experienced at different heights (the crowns of trees versus trunks), but is less significant for the mainly uniform obstacle arrays considered in experimental studies of urban dispersion, such as considered in this paper.

[6] This highlights a particular advantage of the distributed drag approach, whereby variation in canopy density and consequently variation in canopy drag can be explicitly incorporated in the formalism, whereas for simple empirical models such as the UDM, a particular value had to be selected *a priori*.

[7] While the equations for ϵ, such as (15), and that derived in section 3.1, produce broadly correct canopy drag behaviour, they do not capture all subtleties created by non-linear effects of currents between buildings. This is a case of a practical approximation being made in order to generate results that can be tractably used and that are relatively universal compared to CFD calculations of the drag.

[8] This array is like the regular cubical obstacle array discussed in the Coanda data-set (see Section 4), but with the cubes replaced by cylinders.

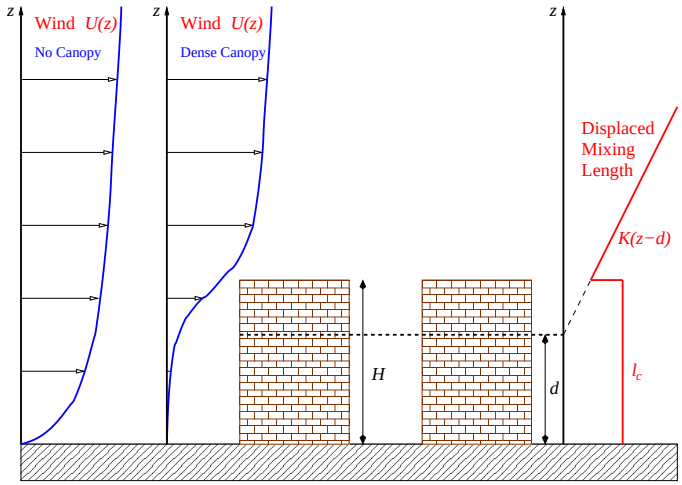

Figure 1: *Effect of a canopy on the wind profile and the resultant model of the mixing length profile l_m. The wind profile above the canopy is approximately the wind profile above a smooth surface, lifted by d, as in (7).*

$T_{ij} \sim K(\partial v_i/\partial x_j)$, and variations of K-ϵ turbulence models can be employed for closure (for details see [13, 14, 15, 16, 17, 18, 19, 20]). Among the variety of available closures, the mixing length hypothesis has been widely adopted on the grounds of its simplicity even though "the assumptions behind this hypothesis are rarely met" [17].

In the mixing length approach, the whole complexity of the turbulent flow parameterisation is reduced to a heuristic model for the mixing length function $l_m(z)$. The mixing layer approach has some justification in the case of a boundary layer over a flat smooth plane where it produces a very close match to experimental data, but it is evident that by its definition the mixing length profile is not a generic property and it may be very canopy specific. It is also very different for sparse and dense canopies: in a dense canopy the turbulent flow in the ABL cannot penetrate deeply into the canopy and affect the mixing process near the underlying surface, while in a sparse canopy mixing near the surface is similar to that of a free surface. Below are some examples of the models for l_m employed in [13, 14, 15, 16]. The profile

$$\frac{1}{l_m} = \frac{1}{Kz} + \frac{1}{l_c}, \quad l_c = \text{const} \tag{17}$$

was used for an urban area where the K used in the literature is a non-dimensional constant, and

$$l_m = (z - (2/3)H)K, \ z/H > 1, \tag{18}$$

$$l_m = \text{const}, \ z/H < 1 \tag{19}$$

for plant canopies (see Figure 1).

An interesting result was recently report by Coceal *et al* [14], where the function of $l_m(z)$ was *a posteriori* evaluated from the canopy flow calculated by Direct Numerical Simulation (DNS—where all scales of turbulence are explicitly resolved in the numerical

solution of the NS equation). The linear sections of the function $l_m(z)$ were evident in their results (see Figure 21 of [14]), it is claimed that in these regions the boundary layer profile can be represented in the "displacement" form (7). Various approximations of the l_m profile presented in Figure 1 can be used for more plausible models of the mean flow in a canopy array in the mixing length parameterisation approach. In dense canopies the variability of the bottom part of the profile disappears since here l_m is constant for $\epsilon \ll 1$ (see (19)). In Section 3, the mixing layer profile l_m based on our model of the mean flow in the canopy is calculated.

Invoking the mixing length hypothesis with $l_m = \text{const}$ allows an analytical solution for the velocity profile near the top of the dense canopy ($\epsilon \gg 1$) that is known as Cionco's canopy profile [21]: $U(z) \sim \exp(cz)$ with c a constant. This profile is used in the UDM as a mean flow profile in the canopy. It is worth noting that while Cionco's profile describes well the flow near the top of the canopy, it violates the boundary condition on the underlying surface ($U(0) \neq 0$), and this can be justified only for a dense canopy.

Another approach to deriving analytical solutions of (13) is to employ various hypotheses of the functional relation between K and U in the canopy. Such hypotheses are usually more generic than the simple mixing length approach since they are, by definition, universal and non-local (contain no explicit dependencies of space coordinates or canopy shape). For instance, the closure $K \sim U$ leads to Cowan's profile: $U(z) \sim \sqrt{\sinh(Az)}$ [38] with A a constant. The Cowan's velocity profile meets the boundary condition at the bottom of the canopy and we will use Cowan's profile as an universal flow model in the canopy. In Section 3.1 we extend Cowan's profile for the mean velocity profile in the ABL for a linear K–U relationship that is valid for dense and sparse canopies (i.e. for large and small values of ϵ), determining the constants of the model in terms of the canopy density.

The important aspect of realistic models of turbulent diffusion in the ABL is to cater for the ABL stability effects. These effects are usually incorporated in dispersion models based on the Monin-Obukhov similarity theory. According to this theory, the stability effects can be accounted for by alteration of mean velocity profiles in the following way:

$$u(z) = U(z) - \phi_m\left(\frac{z-d}{L}\right) + \phi_m\left(\frac{z_0-d}{L}\right), \tag{20}$$

where L is the so-called Monin-Obukhov length scale (i.e. the scale of turbulent flow with thermal fluxes), $\phi_m(z)$ is a known dimensionless function [4, 17], and $U(z)$ is either of the profiles (1) or (2). This considerably complicates the ABL flow problem, and will not be further considered in the current report, but is a challenging extension for a more general model than that discussed in Section 3.1, and will be developed in future work. Progress for plant canopy models has also been recently made by Harman and Finnigan [17].

2.2 Mean Concentration Field

The equation for mean concentration C is a well-known equation of the pollutant budget in K-theory [4, 22]:

$$U(z)\frac{\partial C}{\partial x} = \frac{\partial}{\partial y}\left(K_{yy}(z)\frac{\partial C}{\partial y}\right) + \frac{\partial}{\partial z}\left(K_{zz}(z)\frac{\partial C}{\partial z}\right), \tag{21}$$

with the assumption that

$$K_{yy}(z) = \frac{1}{2}U(z)\frac{\mathrm{d}\sigma_y^2(x)}{\mathrm{d}x},$$

and $\sigma_y(x)$ is the horizontal plume spread. It is known [4, 5, 6, 22, 23] that for power-law profiles and a source on the ground that this equation provides the analytical solution for the pollutant concentration in the surface layer. The solution can be written in the form

$$C(x, y, z) = C_y(x, y)C_z(x, z). \tag{22}$$

The horizontal transverse mean concentration profile C_y has a Gaussian solution

$$C_y(x, y) = \frac{1}{\sqrt{2\pi}\sigma_y}\exp\left(-\frac{y^2}{2\sigma_y^2}\right), \tag{23}$$

where $\sigma_y \equiv \sigma_y(x)$ is the lateral dispersion parameter. The vertical mean concentration profile C_z has a stretched exponential solution

$$C_z = C_0(x)\exp\left(-B(x)\zeta^\alpha\right). \tag{24}$$

Here

$$C_0(x) = \frac{Q}{u_0 z_0}\frac{\alpha}{\Gamma(\beta)}(B(x))^\beta, \tag{25}$$

$$\zeta = \frac{z}{z_0},\ B(x) = \frac{x_0}{x},\ x_0 = \frac{u_0 z_0^2}{\alpha^2 K_0},\ \beta = \frac{1+m}{\alpha}, \tag{26}$$

and $\alpha = 2 + m - n,\ u_0 = a u_*,\ \Gamma(\beta)$ is the Gamma function, and Q is the rate at which the source releases the pollutant (rate of injection). The analytical solution (22), (23) and (24) is a foundation for our model. In Section 4.5 we comprehensively validate it against our experimental data.

For conjugate (5) or Monin-Obukhov (6) profiles we have simple estimates

$$\alpha_c = 1 + 2m, \tag{27}$$

$$\alpha_{MO} = 1 + m. \tag{28}$$

For small α (neutral conditions) these estimates are very close, but in general the following inequality seems to hold: $\alpha_{MO} < \alpha < \alpha_c$. This estimate will be validated based on our experimental data-set (see Section 4.4).

One of the important properties of pollutant dispersion in the ABL described by solution (22) is its universal scaling, i.e. the simple functional relations between its parameters:

$$\sigma_z \sim \sigma_y \sim \mu, \tag{29}$$

where μ is the plume centroid position in the vertical direction (the centre of gravity of the concentration distribution). Such scaling can be justified based on properties of flow in the ABL [22] and can significantly simplify expressions (23) and (24), reducing them to a self-similar universal form in dimensionless variables.

The solution (22), (23) and (24) can be generalised for an elevated source of height $z = H_s$ [4, 22, 23]. In such cases $C_y(x, y)$ will not change, but $C_z(x, z)$ can be written in the form

$$C_z = C_0(x, \zeta)\exp(-B(x)(\zeta_0^\alpha + \zeta^\alpha))I_{-\nu}(2B(x)(\zeta\zeta_0)^{\alpha/2}), \tag{30}$$

$$C_0(x,\zeta) = \frac{Q}{u_0 z_0}(\zeta\zeta_0)^{\alpha\nu/2}\alpha B(x), \tag{31}$$

where

$$\zeta(z) = \frac{z}{z_0}, \quad \zeta_0 = \frac{H_s}{z_0}, \quad B(x) = \frac{x_0}{x}, \quad x_0 = \frac{u_0 z_0^2}{\alpha^2 K_0}, \quad \nu = 1 - \frac{(1+m)}{\alpha}, \tag{32}$$

$\alpha = 2 + m - n$ as above, and $I_\nu(z)$ is the type I modified Bessel function. It is worth noting that parameter ζ_0 (source elevation) is responsible for the vertical concentration profile variability close to the source, and its contribution diminishes at $x > H_s$. It can be shown that at the limit $H_s \to 0$ (i.e. $\zeta_0 \to 0$) this solution tends to (24).

For the solutions given by (24) or (30), the pollutant concentration on the surface ($\zeta = 0$) is given by

$$C(\xi) = \frac{D}{\xi^\gamma}\exp(-F/\xi), \tag{33}$$

with $\xi = x/x_0$ and D, F constant. We can see that function $C(\xi)$ increases from zero, reaches its maximum, and then decays as a power-law. The exponent γ of power law decay is determined by the velocity profile (i.e. exponent m). For the conjugate profile the exponent γ is given by

$$\gamma = \frac{1+m}{1+2m}. \tag{34}$$

It should be noted again that the value of m and hence γ is also influenced by the type of canopy and the stability conditions.

In the UDM framework, a Gaussian form is used for the concentration profile, i.e. simply $\alpha = 2$ in (24) or (30), and the surface reflection is included for elevated sources [1]. This simply leads to $\gamma = 2$ in (33) and any dependency of γ on wind shear disappears. This significantly deviates from the stretched exponential model (24) and (30), even in the neutral case, since by (34) $\gamma \approx 1$ for $m \ll 1$. This may result in possible underestimation of downstream concentration levels predicted by UDM, mostly at far distances from the source. This deviation will only increase if we take into account stability conditions and canopy effects, since they correspond to the higher values of m causing γ to further decrease and to approach its limiting value $\gamma \approx 1/2$ following from (34). Hence the effect of wind shear may be very important for CBR concentration prediction and should be taken into account for high fidelity dispersion modelling.[9]

3 Development of a New Plume Model

3.1 Flow in the Canopy

In Section 2.1 the atmospheric velocity and diffusivity profiles within the ABL were discussed for the case with very little or no canopy to impede the flow based on (1) and (2).

[9]This effect may not be noticeable in the urban modules of the Hazard Prediction and Assessment Capability (HPAC) of which UDM forms a component, as when the plume reaches about 1 km or 10-12 obstacle rows downwind of the source, UDM passes puffs off to the far field dispersion model SCIPUFF. Another complication in this comparison is that UDM is a *puff model*, and thus though the vertical profile of puffs may not be optimal according to the gradient–diffusion theory described here, an aggregation of hundreds or thousands of puffs in a computational domain may not lead to the simple ξ^{-2} dependency for $C(\xi)$ given by the *plume* framework of (33).

The case of wind flow above a significant canopy was also discussed, viz. (7) and (8).

Here the canopy wind flow model of Cowan [38] is extended to create a self-consistent model for the full profile, both within and above the canopy. The aim in the development of this model is to employ as few heuristic assumptions as possible, and for the model to be dependent on as few external parameters as is physically reasonable. Supporting experimental evidence is given in Section 4.4.

The key to modelling average velocity flow within a canopy is to study the shear stress within the canopy, caused by the drag the canopy exerts on the flow [38, 24, 25]. In this way, we can derive a common framework to link equations employed in empirically based and heuristic models such as the UDM, and more physics based distributed drag CFD models described in Section 2.1. The shear stress is given by

$$\tau = \rho K(z) \frac{\mathrm{d}U(z)}{\mathrm{d}z}, \tag{35}$$

where ρ is the fluid density, and $K(z) = K_{zz}$ and U are the average velocity and diffusivity (as in Section 2.1). It is important to note that in the K-theory of dispersion, the assumption of equality between eddy *viscosity* and eddy *diffusivity*, namely $K(z) = K_{zz}$, is automatically made, but this is by no means grounded in rigorous physical theory. We will follow the same approach in this section to enable the formulation of tractable analytic models with minimal fitting parameters, however in general it may be assumed that a constant of proportionality other than unity exists.

The rate of change of shear stress through the canopy can be related to the drag by

$$\frac{\mathrm{d}\tau(z)}{\mathrm{d}z} = \rho \bar{C}_D A U^2(z), \tag{36}$$

where

$$A = \frac{A_f}{A_t H} = \frac{\lambda_f}{H} \tag{37}$$

is the area density (the amount of area perpendicular to the flow per unit volume). It is assumed that the area density is constant in z, a reasonable approximation for an urban canopy. Assuming self-similarity between $U(z)$ and $K(z)$ within the canopy[10] [25] gives

$$K(z) = \sigma H U(z) \tag{38}$$

for canopy height H, with σ a dimensionless parameter to be determined by the model (see below). This leads to the following differential equation describing how drag affects velocity within the canopy:

$$\frac{2\epsilon}{\sigma H^2} U^2(z) = 2 \left(\frac{\mathrm{d}U(z)}{\mathrm{d}z} \right)^2 + 2U(z) \frac{\mathrm{d}^2 U(z)}{\mathrm{d}z^2}. \tag{39}$$

Here we see the re-emergence of the parameter ϵ defined in (15) in a slightly different form, namely $\epsilon = \bar{C}_D \lambda_f$. This different form is due to the use of a bulk drag coefficient

[10] By self-similarity here we mean that $K(z)$ is globally dependent on $U(z)$, and not varying in its dependency in different areas of the canopy. This is a strong assumption, and necessarily approximate, but facilitates the simple but powerful analytical model developed in this section.

$\bar{C}_D$, rather than a series of coefficients in horizontal slices (C_D varying with z). By setting $\chi = U^2(z)$ and $\beta = 2\epsilon/\sigma$, the differential equation reduces to the simple form

$$\frac{\mathrm{d}^2\chi}{\mathrm{d}z^2} - \frac{\beta^2}{H^2}\chi = 0. \tag{40}$$

The solution of this equation is straightforward:

$$\chi(z) = c_1 \sinh\left(\frac{\beta z}{H}\right) + c_2 \cosh\left(\frac{\beta z}{H}\right).$$

This is solved in conjunction with the no-slip condition $U(0) = 0$, which leads to $c_2 = 0$. The resulting solution for U becomes

$$U(z) = u_H \left(\frac{\sinh(\beta z/H)}{\sinh(\beta)}\right)^{1/2}, \quad z < H. \tag{41}$$

We now turn our attention to the flow profile above the canopy, ignoring the local scale structural complexity of the roughness sub-layer (in the spirit of the distributed drag approach), thereby automatically describing this layer and the constant stress layer above in one uniform framework. Following [25], we generalise (1) for velocity above the canopy by introducing an effective canopy displacement height d and roughness thickness z_0:

$$\begin{aligned} U(z) &= \frac{u_*}{\gamma\kappa}\log\left(\frac{z-d}{z_0}\right), \quad z \geq H, \\ K(z) &= \gamma\kappa u_*(z-d), \quad z \geq H. \end{aligned} \tag{42}$$

The diffusivity profile is chosen such that the shear stress (35) above the canopy is a constant. The dimensionless constant γ is a deformation parameter, capturing the departure of the vertical profiles to that of a surface without a canopy. It is to be determined either experimentally or on physical grounds (see [25, 26, 27]; $\gamma \approx 1.5$ in [25]). We expect that all our equations should be valid (at least approximately) for a value $\gamma = 1$, which is assumed below unless otherwise specified. This is in keeping with our philosophy of not introducing extra empirical and tunable parameters that are difficult to specify in a robust manner. However it is clear that in reality *gamma* will vary with different canopies, and this will be explored in future work.

In a similar way to [25], to determine the unknowns σ, u_H, d and z_0, we can introduce four physically reasonable boundary conditions, which match the canopy and above-canopy profiles:

$$\begin{aligned} U_+(H) = U_-(H), \quad & \left.\frac{\mathrm{d}U_+(z)}{\mathrm{d}z}\right|_{z=H} = \left.\frac{\mathrm{d}U_-(z)}{\mathrm{d}z}\right|_{z=H}, \\ K_+(H) = K_-(H), \quad & \left.\frac{\mathrm{d}K_+(z)}{\mathrm{d}z}\right|_{z=H} = \left.\frac{\mathrm{d}K_-(z)}{\mathrm{d}z}\right|_{z=H}. \end{aligned} \tag{43}$$

Here the $+$ and $-$ subscripts denote the "upper" and "lower" formulae, valid above and below $z = H$ respectively. These conditions enforce the continuity and smoothness of $U(z)$ and $K(z)$ at height H. The last condition, imposing smoothness of $K(z)$ is new, and

is required as the advection diffusion equation (21) used to find the plume concentration explicitly involves the first derivative of $K(z)$.[11]

Solutions (41) and (42) are matched with the boundary conditions (43) to give the following relationships:

$$\frac{d}{H} = 1 - \frac{\sigma}{(\gamma\kappa)^2}, \tag{44}$$

$$\frac{z_0}{H} = \frac{\sigma}{(\gamma\kappa)^2 e^1}, \tag{45}$$

$$\frac{u_H}{u_*} = \frac{1}{\gamma\kappa}, \tag{46}$$

$$\tanh\left(\sqrt{\frac{2\epsilon}{\sigma}}\right) = \frac{1}{(\gamma\kappa)^2}\sqrt{\frac{\epsilon\sigma}{2}}. \tag{47}$$

Equations (44) and (45) lead to the useful relationship

$$\frac{d + z_0}{H} = 1 - \frac{\sigma}{(\gamma\kappa)^2}(1 - e^{-1}). \tag{48}$$

In this analysis $\epsilon \to \infty$ corresponds to an infinitely dense canopy and $\epsilon \to 0$ to an infinitely sparse canopy.

The resulting behaviour of the velocity profile is given in Figure 2 for the cases of a relatively sparse canopy and for a dense canopy. In the sparse canopy, the wind momentum penetrates the canopy deeply, so the drag is applied directly to the underlying surface. In the opposite case of a dense canopy, very little wind reaches the surface, so most of the drag is absorbed by the canopy elements.[12] In general our velocity profile is similar to the one found by DNS in [14].

It is readily seen that as $\epsilon \to \infty$, (47) implies

$$\sigma \to \frac{2(\gamma\kappa)^2}{\epsilon},$$

and thus

$$\begin{aligned} d + z_0 &\to H, \\ d &\to H, \\ z_0 &\to 0. \end{aligned}$$

It should be noted that this limit could be expected to be identical to that with no canopy, but raised by height H. Substitution shows this is not the case, and is an artifact of holding the velocity constant and non zero at the canopy top (height H) while matching

[11] It should be noted that the analysis prior to the imposing of these boundary conditions is identical to that by Cowan in [38]. However Cowan does not impose smoothness at the boundary. It is the addition of the expanded boundary conditions of the first derivatives used here that allows the determination of the key flow parameters d and z_0 in terms of canopy density necessary to make the model more analytic.

It was only realised after the fact that some of this model had been previously derived in [38].

[12] This is validated for our model by studying the shear stress at the ground as a function of parameter ϵ (see Figure 3).

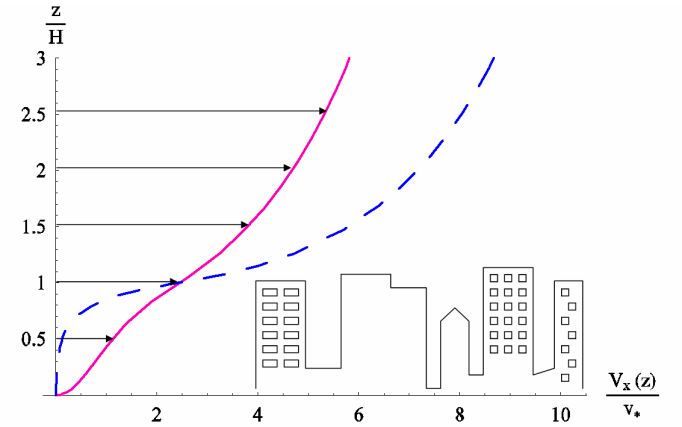

Figure 2: *Average horizontal velocity profile. The pink/solid line is for a sparse canopy ($\epsilon = 0.5$, typical urban) and the blue/dashed line for a dense canopy ($\epsilon = 2$, forest).*

parameters between the canopy wind profile and the wind profile above it. This shall be explored and corrected in a future paper.

In the opposite limit $\epsilon \to 0$

$$\begin{aligned} \sigma &\to 2(\gamma\kappa)^2, \\ d + z_0 &\to 2(e^{-1} - 1)H, \\ d &\to -H, \\ z_0 &\to 2He^{-1}. \end{aligned}$$

The main feature of the limit $\epsilon \to 0$ is independency of the parameters d and z_0 from ϵ, so their behaviour is universal. Unfortunately, the skill of our model in predicting the limits $d(\epsilon = 0)$ and $z_0(\epsilon = 0)$ are not very advanced and needs further improvement in these extremes (future work will be based around the approach of Appendix A.1). It should be noted that the expected values for $d(\epsilon = 0)$ and $z_0(\epsilon = 0)$ are 0 and the viscous length scale[13], respectively.

The plots of equations (44) and (45) showing d and z_0 as functions of ϵ are presented in Figure 3a. It is interesting to compare these plots with the empirical plots and formulas used in the UDM—see (11), (12) and Figure 25 of [1]. Since ϵ is proportional to λ_f the agreement between the results for $\epsilon > 1$ (for dense canopies) is satisfactory. In the limit of the sparse canopy $\epsilon \ll 1$, the agreement is not visually good, since this limit involves some ambiguity (for a discussion see Appendix A.1). However away from the sparse canopy extreme, the $U(z)$, d and z_0 profiles are quite reasonable and agree well with experiment (see Section 4.4). The lower limit of ϵ for which we can use this theory without much concern is determined by when $d = 0$. The corresponding threshold value of ϵ is $\epsilon \approx 0.3$, which is smaller than typical values found for canopies considered in this report (see below).

[13]This is a lower bound placed upon the roughness length, as viscosity creates effective roughness even for perfectly smooth surfaces. Usually this effect is swamped by the presence of canopy objects.

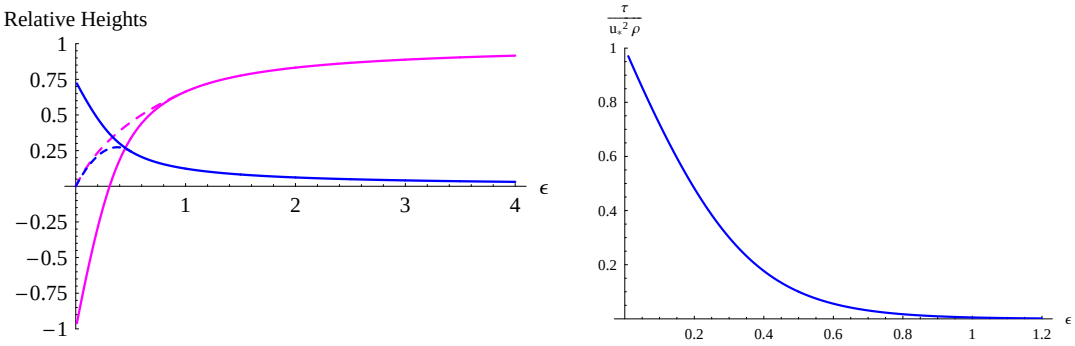

Figure 3: **Left - Pink:** *Relative displacement height d/H as a function of canopy drag parameter ϵ (solid pink line). That $d < 0$ for $\epsilon \to 0$ is an artifact of the functional form imposing a behaviour change in flow at height H, even for an infinitely sparse canopy. This is remedied by letting $H \to 0$ as $\epsilon \to 0$. The dashed pink line is a sketch of d corresponding to the UDM (11).* **Left - Blue:** *Relative roughness height z_0 as a function of canopy drag parameter ϵ. Similarly to d, the fact that $z_0 \neq 0$ for $\epsilon \to 0$ is an artifact of the functional form imposing a behaviour change in flow at height H, even for an infinitely sparse canopy. This is remedied by letting $H \to 0$ as $\epsilon \to 0$. The dashed blue line is a sketch of z_0 corresponding to UDM (12).* **Right:** *Plot of wind shear stress at ground level computed with the proposed model. We see a clear monotonic decrease of surface shear stress with the canopy density ϵ, as intuitively reasoned on physical grounds.*

For model consistency it is enlightening to study the shear stress at ground level, given by (35) and plotted against canopy density ϵ in Figure 3b. As seen in this plot, for very sparse canopies, the shear stress is concentrated at the ground, whereas for dense canopies, the wind does not penetrate to the ground and there is practically no shear stress there, as is required on physical grounds. Examining Figure 3, we can claim that for our model all canopies with $\epsilon > 0.8$ can be considered dense.

It is interesting to calculate the mixing length l_m used by other models—e.g. (18) and (19) discussed in Section 2.1—based on our framework. The formula for l_m is

$$l_m = \kappa \frac{U(z)}{U'(z)},$$

and l_m is plotted for sparse and dense canopies in Figure 4. This can be compared to plots for l_m found in the work of Coceal *et al* [14] (Figure 21 of that paper). The general trend of our profile of l_m matches the results of the other models in key features, such as that l_m increases sharply for $z > H$, and is non-zero within the canopy.

3.2 A New Model for the Mean Concentration Profile

The new model presented in the previous section for flow in and above a canopy, combined with the universal solutions for the mean concentration profile in a shear flow (24) and (30) lay the ground-work for a new model of concentration profile in the ABL with a canopy. The key points to this model are:

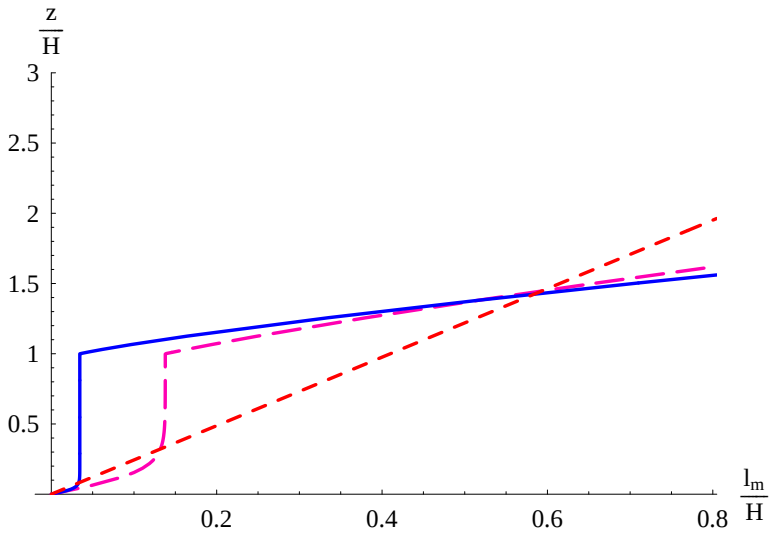

Figure 4: *Plot of mixing length l_m for our flow model. The pink (long dashed) and blue lines are for $\epsilon = 1$ and 4 respectively. The red (short dashed) line is to give a comparison of the gradient of Figure 21 in [14] for $z > H$.*

1. Since the mean flow above the canopy (42) can be modelled with the two parameters d and z_0, expressed in Section 3.1 in terms of canopy density ϵ and height H through (44), (45) and (47), the power-law velocity profile (8) with the same value of these parameters is also a realistic model of the mean flow in the canopy[14]. For this power law profile, the stretched exponential solutions for concentration (24) and (30) are exact solutions of the turbulent diffusion equation (21), so we come to the conclusion that the formula (30) should be a realistic model of concentration distribution for $z \geq d$, if ζ is replaced by $\zeta = (z - d)/z_0$, where d is the height that the canopy has displaced the plume by, and is defined by our flow model (see Figure 1). We acknowledge that the new model for canopy flow derived in the previous section, which uses a log law profile, is mathematically inequivalent to the power law profile employed to derive the vertical mean concentration distribution, and thus the models are in some sense incompatible. However as shown in Section 2.1, within the ABL the two models are similar enough to be interchangeable. Thus we take a practical approach here that employing these different velocity functions for different purposes is the only way to make progress in deriving simple analytical models in the first instance.

What is the concentration distribution for $z < d$? The simplest assumption is to assume that far from the source the flow in the canopy is well-mixed and is in dynamical equilibrium (all concentration gradients have been smoothed out by turbulent diffusion). This leads to the conclusion that

$$C_z(x, z) \approx C(x, d), \quad z < d. \tag{49}$$

This "clipped stretched exponential" profile is a good approximation everywhere outside

[14]There is a cost to taking this equivalence, in that the power law profile is not universal, and introduces constants which will need to be fitted by comparison to experiment, however this a traded off against a functional form of the velocity profile for which analytic plume concentration calculations are possible.

the the so-called source region, which is typically one to two obstacle rows downstream in the obstacle arrays considered in this report and other similar studies. A supporting analytical argument can be found in Appendix A.2.

2. An alternative model to the "clipped stretch exponential" model (49) can be formulated in terms of the power-law exponent α in (24).

In Appendix A.2 it is shown that near the bottom of the canopy the advection-diffusion equation can be solved to give a mean concentration profile with $\alpha = 2$. Thus a smooth, continuous function for the concentration profile can be arrived at by assuming:

$$\begin{aligned} \alpha &= \alpha_0(1 - \lambda \exp(-z/d)), \\ \lambda &= 1 - 2/\alpha_0 \end{aligned} \tag{50}$$

and inserting this into mean concentration profile (24). The ansatz for α has been designed to change behaviour at the effective canopy height d.

Conceptually, close to the ground this model predicts that the effect of the canopy is to restrict the wind and to cause the tracer to disperse in a Gaussian manner. Then above the canopy, the dispersal is dictated by the power law behaviour of the wind and diffusivity functions. In Section 4.5 this model is validated against our experimental data-set and provides a close match.

It should be emphasised that the vertical dependency of α introduced in (50) will modify not only the power-law exponent in concentration formulae (24) and (30), but also the pre-exponential term C_0, which contains α within x_0. From physical grounds, such complex modification of the concentration profile is imposed by the self-similarity property of the solutions (24) and (30).

3. The next new feature of our model is an "effective elevation" of the tracer source, i.e. non-zero value of the parameter ζ_0 in (30), even for ground-level sources. The physical reasoning behind this is an observed effect of the mean flow being pushed up by the canopy. This is coupled with the effect of the highly turbulent recirculation region behind the obstacle where the source is placed, rapidly mixing the tracer to fill the entire wake up to the canopy height with contaminant. This effect is most pronounced when the source is placed just in front of a canopy object. Such effects have been observed in many previous obstacle dispersion experiments [7, 12, 28, 34, 36]. The experimental evidence for this with the currently considered data-set is covered in Section 4.5.

The resulting pattern of the pollutant is as if it were released from an elevated source (Figure 13 below gives an example of this effect from our data). Including a non-zero parameter ζ_0 in our model for ground-level sources permits a realistic description of the vertical variability of the concentration profile in the "near source" field before the concentration distribution approaches the "clipped stretched exponential" regime described above.

It is possible to provide a simple estimate of the value of ζ_0 in terms of the relative source position and the averaged canopy height H for ground level sources within the canopy. It is evident that $0 \le \zeta_0 \le 1$, so as the first approximation we can take

$$\zeta_0 = (H - \sigma_{z0})/H, \tag{51}$$

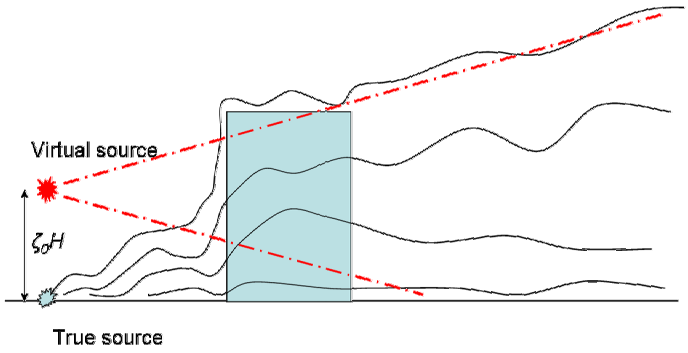

Figure 5: *Illustration of the concept of a virtual source induced by the wake regions of the obstacle array. The virtual source is lifted to height $\zeta_0 H$ (52).*

for $\zeta_0 \leq 1$ and $\zeta_0 = 0$ otherwise (see Figure 5). The plume spread σ_{z0} is the corresponding vertical dispersion parameter taken if no canopy were present,[15] and can be estimated from the well-known kinematic condition [4] $\sigma_{z0} \approx V_\perp x/V_\parallel \approx u_* x/U_0 \approx C_f x$, where u_* is the friction velocity, U_0 is the undisturbed velocity far from the surface (at the top of the boundary layer) and C_f is the drag coefficient for the flow over a flat smooth surface [4]. Thus we obtain

$$\zeta_0 = (H - \psi C_f X_H)/H, \tag{52}$$

where X_H is a distance from the source to the first canopy element downstream and ψ is a numerical factor to be determined.

To summarise the urban plume model discussed above, we have $C_y(x, y)$ unchanged from (23), and combining the elements above, we obtain the following model for $C_z(x, z)$:

$$C_z = \begin{cases} C_0(x,z)\exp(-B(x)(\zeta_0^\alpha + \zeta^\alpha))I_{-\nu}(2B(x)(\zeta\zeta_0)^{\alpha/2}), & \text{if } z \geq d \\ C_z(d), & \text{if } 0 < z < d, \end{cases} \tag{53}$$

$$C_0(x,\zeta) = \frac{Q}{u_0 z_0}(\zeta\zeta_0)^{\alpha\nu/2}\alpha B(x), \tag{54}$$

$$\zeta(z) = \frac{z-d}{z_0}, \qquad B(x) = \frac{x_0}{x}, \tag{55}$$

$$\zeta_0 = \frac{H - \psi C_f X_H}{H}, \qquad x_0 = \frac{u_0 z_0^2}{\alpha^2 K_0}, \qquad \nu = 1 - \frac{(1+m)}{\alpha}. \tag{56}$$

Including the varying α hypothesis instead of a having constant behaviour below d is also possible, but leads to complications that will be resolved in future. Instead, in the next section, varying α is studied without an effective source rise.

The verification of the components of this model is discussed in the following section.

[15] Thus not to be confused with the actual plume spread derivable from the canopy model being discussed.

4 Data Analysis

4.1 Introduction

The plume dispersion models described in this report do not give self-contained predictions of the contaminant concentration fields. Instead they predict the functional form of the concentration distributions based on assumptions about the nature of the underlying flow. Analysis of experimental data can validate the assumptions about the flow used to derive the dispersion models. The data can also fix the free parameters of the dispersion models to give predictive power to the models.

The data presented here were collected in water channel simulations carried out in the Coanda Research & Development Corporation's (Burnaby, British Columbia, Canada) environmental water channel. The simulations were conducted in collaboration with Defence Research and Development Canada (DRDC), which had a multi-year program in the development of the channel and collection of extensive velocity and 1-dimensional (1D) tracer dispersion data-sets. DSTO extended the experimental program to investigate 2-dimensional (2D) sampling of the tracer concentration, as well as in-canopy velocity measurements, as described below. The water channel is specially designed for dispersion modelling, and has a working section of 10 m length with a cross section of 1.5 m width and 0.9 m height. We will give a brief description of the water channel experiment here, to establish the context behind the data. Considerably greater details of the water channel experiments and the instrumentation deployed are available in a report provided by Coanda [29], and previously published work using this data [28, 30].

4.2 Brief Experimental Description

The upwind part of the working section of the water channel was used to generate an appropriately scaled model of the neutrally-stratified ABL. A thick rough-wall boundary layer in the water channel of about 0.3 m thickness was generated. The combination of saw-tooth fence and turbulence grid made of square bars 19x19 mm was used to immediately produce some of the larger-scale turbulent eddies in the boundary layer. Downstream of the saw-tooth fence, the floor of the water channel was covered with a black anodised expanded metal mesh of height 4 mm with a total length of 6 m to give a long fetch of surface roughness for the upstream flow development. The flow then encountered either further mesh for the case of open terrain with no obstacles, or the model obstacle array, which was mounted on a turntable that extended 1.25 m in the stream-wise direction. Downstream of the obstacle array, the flow encountered a section covered with the same black anodised expanded metal mesh that was used for the initial upstream approach flow development.

Two approaches were used to measure velocity statistics within the boundary layer of the water channel. A dual-beam laser doppler velocimeter (LDV) fibre-optic probe was used in the original experiments commissioned by DRDC. To complement this data set, DSTO commissioned some acoustic doppler velocimetry (ADV) measurements using a Sontek MicroADV instrument. Both these instruments have their strengths and weaknesses [31], and a combination of the two data sets provides a complete and complementary

set of velocity measurements. Vertical profiles of mean wind and other turbulence parameters were measured in the equilibrium (fully-developed) boundary layer upstream of the obstacle arrays. The height of the boundary layer, taken to be the height where the mean wind was 99% of the free-stream value, was found to be 275 mm. At this point, the mean wind speed was 0.375 m s^{-1}.

For the water channel simulations, a ground-level point source was used, emitting sodium fluorescein dye tracer at a constant flow rate. An example of one particular obstacle array is presented in Figure 6 (left panel). The source was located at the first street canyon, and the measurements were conducted for the various models of urban terrain (obstacle array configurations). The size of the "atomic" cubic element of the various obstacle arrays was $H = 31.75$ mm. A number of Urban Arrays of different heights ($1H$, $2H$, $3H$ and their random combination) and different space patterns (regular and random) were used in the simulations. Measurements in the so-called "Tombstone Array" were also conducted to enable comparison to a similar experiment conducted using 1D line-scans by DRDC. The Tombstone Array was constructed from vertical stainless steel tabs (60x10x1 mm) installed vertically into laser cut slots and arranged in staggered formation. For Urban Arrays, measurements were conducted at six downstream locations ($2.0H$, $4.0H$, $10H$, $16H$, $26H$), and for the Tombstone Array at five downstream locations ($1s$, $2s$, $4s$, $7s$, $12s$, where $s = 44$ mm).

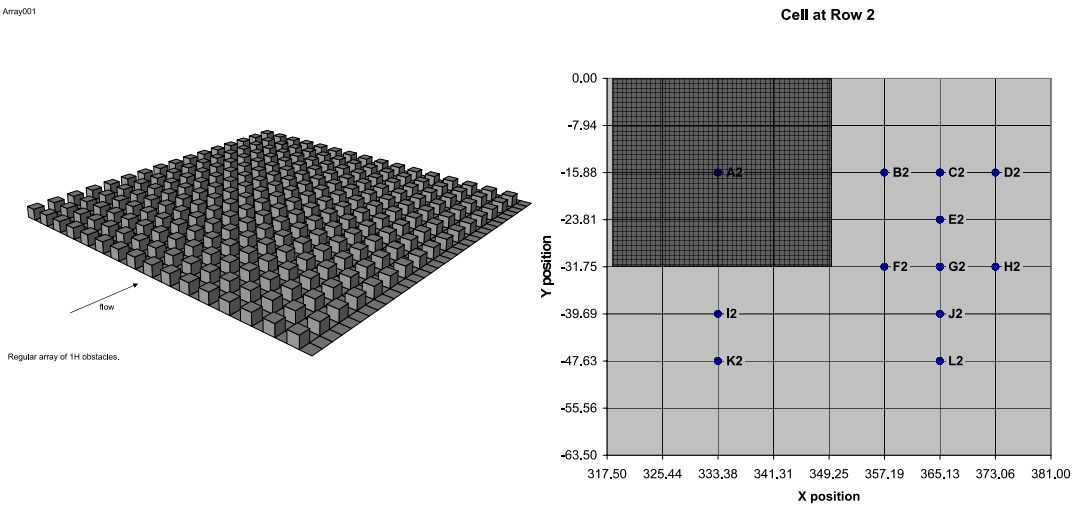

Figure 6: *Left: Coanda Urban Array 001 consisting of regularly spaced cubic objects with packing density 0.25. Right: Location of positions within a cell unit where velocity measurements were taken. The dark shaded area indicates the position of the object within the unit cell.*

The instantaneous concentration field in the dispersing dye plume was measured using the 2D laser-induced fluorescence (LIF) technique, which permitted simultaneous multi-point concentration measurements to be acquired with high spatial and temporal resolution. A fluorescent dye is emitted from a source, and then disperses in the turbulent boundary layer. The dye encounters a laser sheet that causes the dye to fluoresce. Each pixel of the real time fluorescing image can be accurately calibrated to a concentration field and captured in a CCD camera. Each 2D scan consisted of 696x260 pixels, giving a

spatial resolution of about 1.4 mm. The 2D scans were sampled for 1000 s at 23 frames per second, giving data sets of about 23,000 images per experiment.

In addition to low level data, Coanda has also supplied analysis programs and analysed data. A software framework has been developed here at the DSTO to allow the comparison of plume dispersion models and the Coanda data. This software framework utilises the lower-level Coanda software and processed data, and applies higher-level analysis. For preliminary data analysis the software was developed in MATLAB. A more advanced framework is written in the C++ programming language. It provides a convenient environment where large amounts of processed data can be collected and analysed. Software to read and analyse low level Coanda data has also been developed. Fitting and other analyses are performed using the ROOT analysis package [32] developed by the high energy physics community.

4.3 Coanda Dataset—Preliminary Analysis

The Coanda data-set has been used in several studies of plume dispersion [28, 30, 33]. In this report the 2D Coanda data-set is used to validate analytical predictions of the models developed in the previous section. As a first step for such validation, we verify the existence of universal scaling (29) and existence of stretched exponential profiles (24) and (30) in a complex canopy.

According to (29), the ratios σ_y/μ and σ_z/μ should not depend on the downstream position. This fact was demonstrated in a previous paper [30].

Also, that the cross-stream mean concentration is given by Gaussian distribution (23) has been observed in many previous studies [12, 28, 33, 34, 36]. This Gaussian behaviour can be seen in figures 11 and 13.

The stretched exponential solution (24) was used to match the mean concentration profile in the vertical direction for the turbulent surface layer above both smooth and rough surfaces. The results are presented in Figure 7. As can be seen the stretched exponential model is consistent with the measured concentration data.

In Figure 8 the plot of $y = \log(\log(C_{max}/C))$ against $x = \log z$ is presented (smooth surface case), so each stretched exponential profile corresponds to a straight line (with the slope of such a line determined by the power exponent α in (24)). From the left-hand plot, we observe that the stretched exponential function is a plausible model for the mean concentration profile in the vertical direction for the case of a simple sheared boundary layer (all plots collapse under normalised coordinates).

The righthand plot in Figure 8 shows the effect of the regular cubical obstacle array on the standard vertical profile form. We can see that the canopy causes a deformation of the slope around height H, i.e. plot of $\log(\log(C)$ becomes horizontal within the canopy. Because of mixing and flow homogenisation, the value of α tends to 0 in this region. This is consistent with the "clipped stretched exponential solutions" (49) and (53). However we do not use $\alpha \to 0$ to model the concentration profile using a varying α formalism (as in (50)) as this contradicts the result of Appendix (A.2).

From these plots we estimate a value of the α exponent of the stretched exponential distribution for various downstream positions. We find a good agreement between values

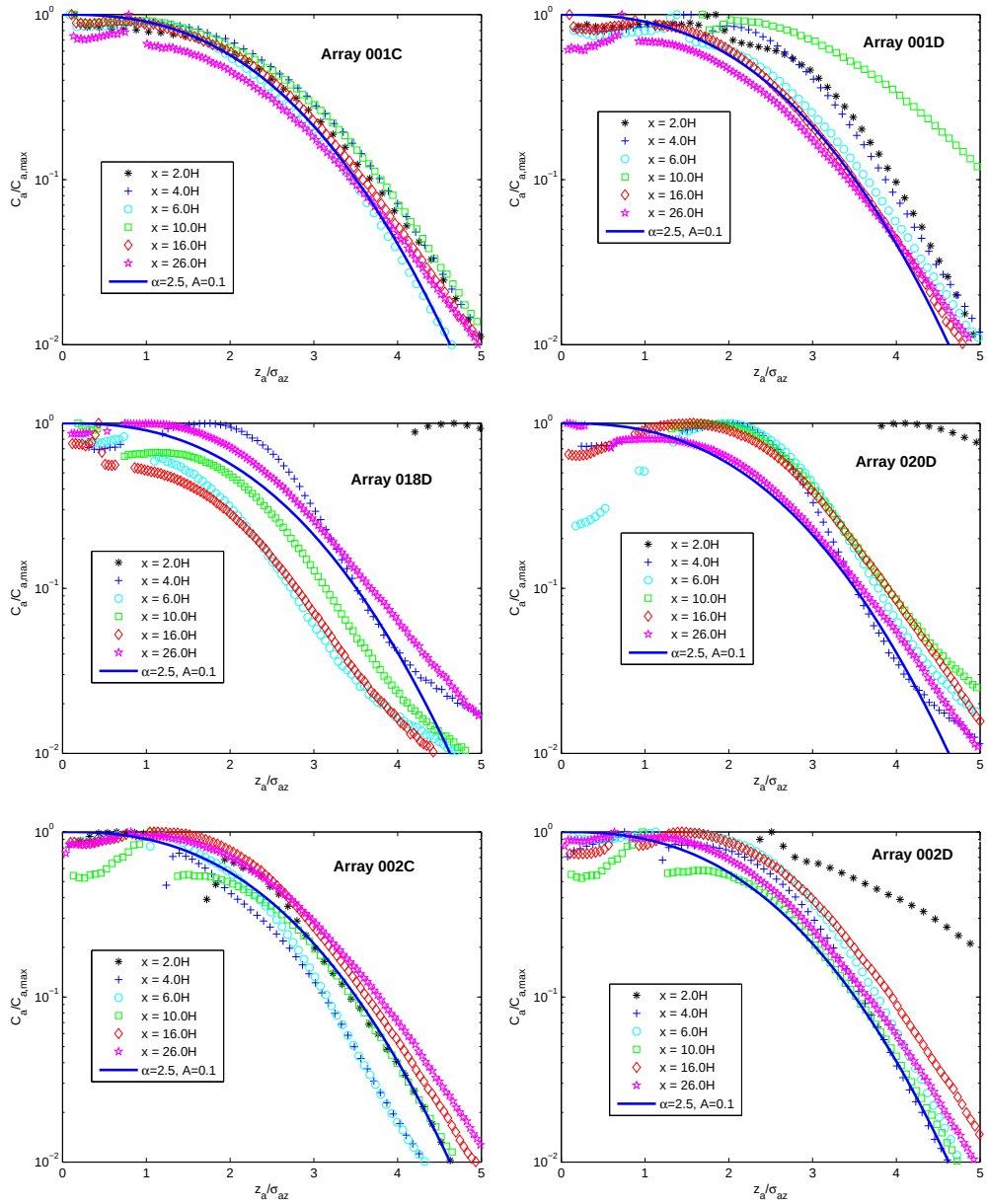

Figure 7: *Vertical cross-sections of the normalised mean concentration as a function of downwind position. Solid line is the stretched exponential fit (24). C_a depicts the time averaged concentration at that height and downstream position, $C_{a,max}$ is the maximum concentration along this vertical axis. σ_{az} is the standard deviation in the vertical position. Description of the obstacle arrays can be found in [29].*

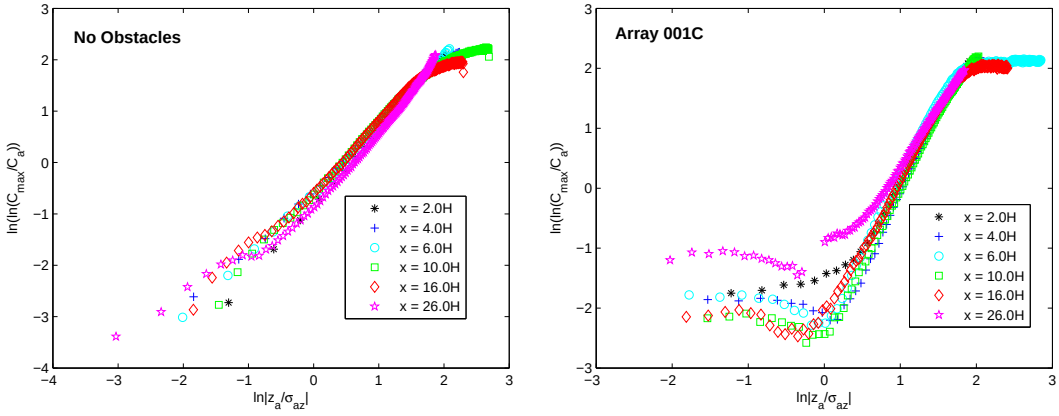

Figure 8: *Plot of* $\log(\log(C_{max}/C_a))$ *against normalised vertical coordinate* $\log z/\sigma_{az}$. *The slopes of curves are determined by the power exponent* α *in (24).*

of α found from data presented in Figure 8. (and plotted in Figure 9) with our theoretical estimates ($\alpha_c = 1 + 2m = 1.54,\ \alpha_{MO} = 1 + m = 1.27$) for a measured value of $m = 0.27$ (obtained from fitting to data in Figure 11).

4.4 Coanda Flow Velocity Measurements

The velocity of the atmospheric flow within and above an urban canopy is the key driver of plume dispersion. For the models described in this report the mean stream-wise velocity and its height dependence are important parameters.

The Coanda data-set includes measurements of the velocity fields over a range of mock urban canopies. Individual data points give a measurement of two of the velocity components at a single point in the flow. With repeated measurements, the full 3-D flow structure can be characterised at a range of heights and positions within and above the canopy.

Figure 10 shows an example of the velocity information that can be extracted from the Coanda data-set. The configuration of the obstacle array for this measurement is designated Urban Array 001. This array consists of a regular pattern of cubic objects as shown in Figure 6. Also shown in Figure 6 (right panel) are the positions within one of the array sub-units where the velocity measurements of Figure 10 were taken. The velocity measurements in Figure 10 show that the flow velocity above the canopy is uniform over the array (ie the data points all follow a common line). That the data points within the canopy have a significant spread in velocities indicates that there are complex flow patterns depending on the location of the measurement with respect to the objects of the array.[16]

[16]It should be noted that the measurement points are not ideally placed for this fit to give a true average of the velocity profile of the system. Rather this plot gives a representative idea of the behaviour of the velocity profile. Negative velocities correspond to eddies directly behind the array objects.

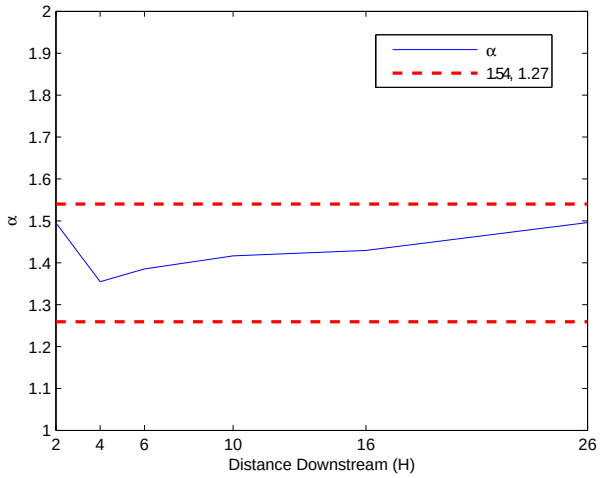

Figure 9: *Variation in the parameter α of (24) as a function of downstream distance from the source for the Coanda data with no obstacles.*

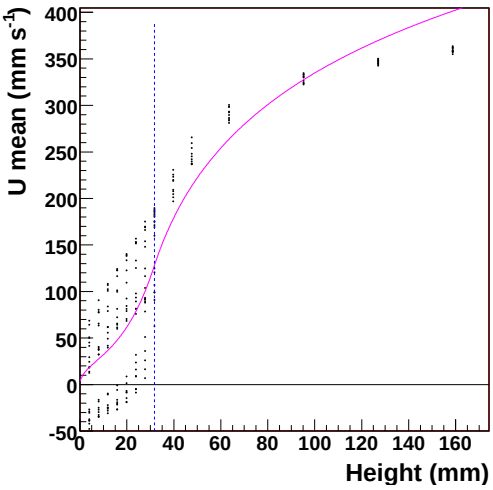

Figure 10: *Measurements of height z vs. mean stream-wise velocity U for the Coanda Urban Array 001. The data points come from measurements at different representative points around a single array object. The configuration of the array and the location of measurement points can be seen in Figure 6 (right panel). The dashed blue line indicates the height of the objects in the array. The solid line is a fit of all of the data to the functional form given in (41) and (42).*

4.5 Coanda Mean Concentration Measurements

As mentioned in the Introduction, the long term goal of the work presented in this report is to find models that can describe the concentration fluctuations in a plume. An important first step in developing these models is to describe the time averaged behaviour of the plume. The basic form of the stretched exponential solution for mean concentration in a plume is shown in (24).

Underlying this solution is the description of the flow, namely that the mean downstream velocity, U, and diffusivity, K vary with with height as a power law. Equation (24) has four free parameters associated with the flow: U and K at a reference height and their respective power law height indexes m and n. If the absolute concentration is not normalised this gives a total of five free parameters. Clearly the number of free parameters is a major difficulty in validating (24). Part of the data analysis work described here has been to maximise the use of available data to constrain the fit parameters.

For the Coanda data-set, the measured concentrations are normalised to a known source strength. Using this information it is possible to fix the absolute concentration normalisation of (24) rather than have it as a fitted parameter. Further constraints can be put on fitted parameters by demanding consistency in the parameters of the flow at different locations. This has been achieved by performing a global fit for flow parameters over plume concentration profiles at different downstream distances from the source.

Figure 11 shows an example of fitting (24) to Coanda data for the case where there is no urban canopy. The figure shows that if the fit parameters are allowed to vary for each profile, the functional form of (24) can provide an excellent match to the data. If a global fit is done, demanding the same flow parameters in all parts of the flow, then the fit, although not perfect, is still a very good description of the data.

Figure 12 shows fits of a stretched exponential form to Coanda data where an urban array is present (Urban Array 001). The presence of the canopy causes a vertical displacement in the flow as discussed in Section 3.2. In Figure 12 the vertical concentration profiles have been fit to the form given in (53), with displacement height d calculated from (44) to be 11 mm. Within the canopy the concentration is assumed to be constant. If the flow parameters are allowed to vary at different locations in the array then the functional form of (53) describes that data well.

If a global fit is done, with consistent flow parameters throughout the array, then the fit works poorly. The reason for this is probably that while the functional form (53) does predict that the amount of material in a plane perpendicular to the direction of flow attenuates with distance from the source[17], the concentration attenuation in the Coanda experiment is much too high to be explained by this effect (the functional form predicts an 8-10% loss between the 508 mm and the 825 mm points, whereas what is lost is closer to 50%). Rather material is apparently being lost because the sensors cannot detect a local concentration below a specific threshold, and thus when a plume fluctuation drives the concentration too low, especially when the average concentration in the region is already low, then the sensor records that no tracer is present. Alternative explanations are that the flow is non homogeneous over the array (quite possible as the array designers put

[17]This is because conservation of concentration flux at the higher wind speeds of greater altitudes corresponds to lower concentrations.

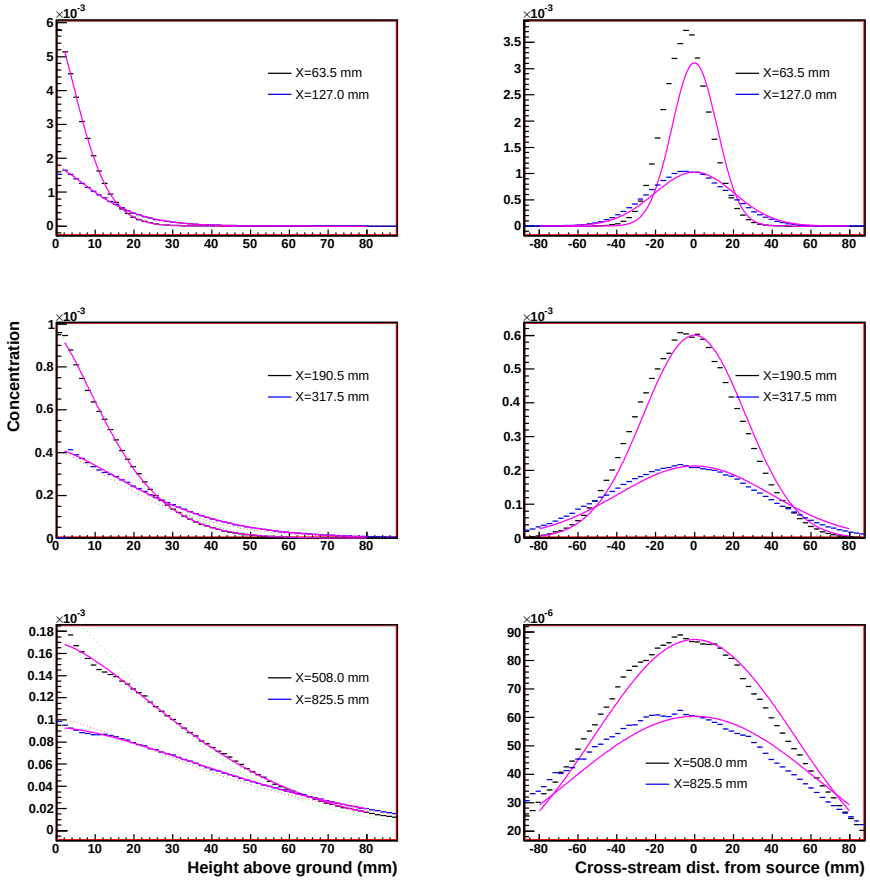

Figure 11: *Plume concentration profiles from Coanda data: a ground level release over flat terrain (no canopy). The plots on the left show the vertical concentration profile at different downstream distances (black and blue points). Concentration has been normalised by concentration of dye in the source pipe fluid and is dimensionless. The plots on the right show the horizontal plume profile. In each plot the magenta line shows the results of fitting (24) (vertical profiles) and a Gaussian function (horizontal profiles) while allowing the flow parameters to vary at each downstream position. The red and green lines in the vertical profile plots show the form of (24) if the fit parameters are derived from a global fit to all vertical concentration profiles.*

1

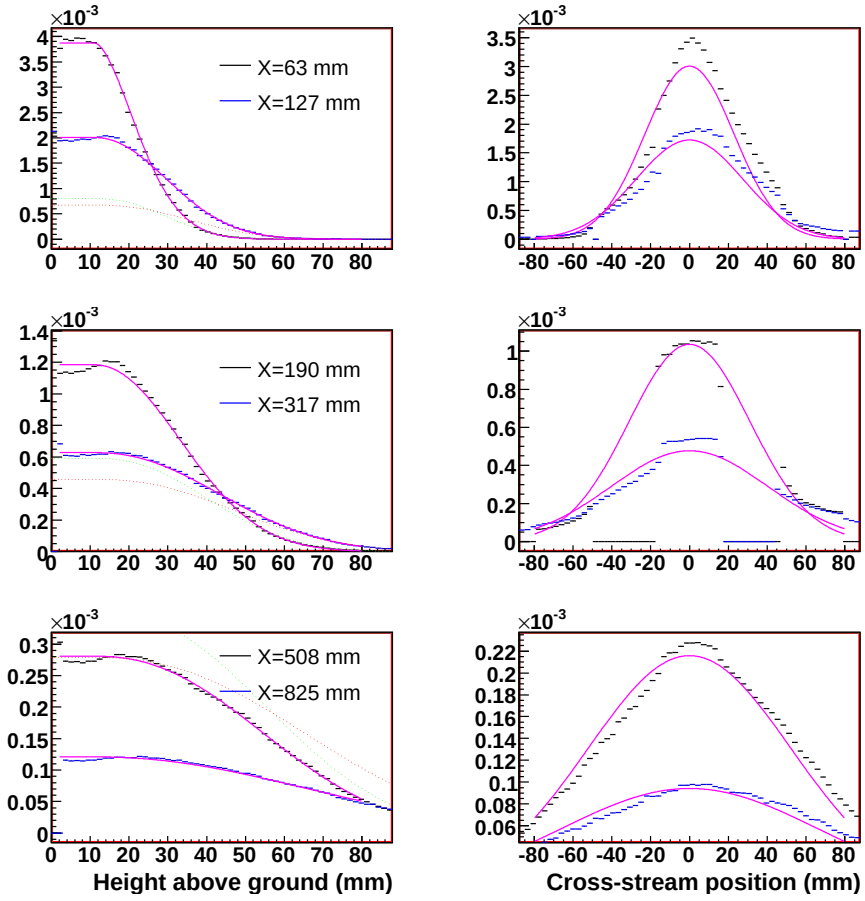

Figure 12: *Same plots as shown in Figure 11, but for plume dispersion over Coanda Urban Array 001. Vertical axis is concentration and has been normalised by concentration of dye in the source pipe fluid and is dimensionless. See Figure 6 for details of this array configuration. The source has been located at ground level in a canyon between rows of objects. The functional form used in the fits is given by (24). The dashed lines in the left hand plots refer to a global fit over all the data.*

the plume sources near the beginnings of the arrays, so turbulent conditions are likely to be different at the source than near the middle) or that the model is missing some key behaviour. Further investigation is required to resolve this.

The vertical displacement of the flow caused by a canopy is an example of a global effect of a canopy on the flow. In the Coanda data we can also see local effects on the plume due to structures in the canopy. Figures 12 and 13 show concentration profiles taken under identical flow and array configurations. The only difference is that in Figure 12 the source was placed in a "canyon" between rows of objects in the canopy, while in Figure 13 the source was placed directly upstream of an object. The vertical concentration profile in Figure 13 shows a pronounced peak that is higher than that seen in Figure 12. We hypothesise that the local structure in front of the source is pushing part of the plume upward simulating a non ground-level source. This type of effect has been observed consistently in previous obstacle array experiments [12, 28, 34, 36]. To fit the data we have used the form of the raised clipped stretched exponential (53) and we have used (44) to calculate the effective canopy height $d = 11\ mm$ and made an ad-hoc assignment of source height of 10 mm[18]. As can be seen, the fit of the functional form to the experimental data is currently faulty. While the functional form can indeed produce the same flat region within the canopy followed by a rise in concentration above the canopy, which fades with distance, the algorithm used in obtaining this plot has not yet been adjusted to account for the effective loss of tracer as discussed for Figure 12. Initial calculations suggest that once this weakness in the experimental data is accounted for, (53) should fit the experimental data well.

The plot in Figure 14 represents a fit with the varying α of equation (50). We observe that this model provides a satisfactory fit in the region close to the source, although slightly worse than for the "clipped stretched exponential" in Figure 12. As expected, the two different functional forms and make mostly no difference above the canopy.

5 Conclusions and Future Work

The high fidelity modelling of tracer dispersion in heterogeneous canopies is a computationally intensive task that still requires long execution time and significant computer resources. In the current report we have shown a new approach for development of simplified flow and dispersion models for urban environments that are easily treated numerically in an operational environment with minimal computer resources. The framework established does not intend to offer a new generation of dispersion models to replace existing operational models, but rather provides a link between empirical, fast models such as the UDM, and computationally intensive CFD models. The models can thus justify some heuristic approximations of the UDM, and provide an important performance check for CFD models. This enables a more comprehensive understanding of the problem, with greater clarity in the approximations and assumptions made for various dispersion models. We have presented experimental results from water channel experiments to support the theoretical findings.

[18] A best guess assignment is used at this stage as the problems with the current global fit algorithm means ψ in (52) is yet to be determined.

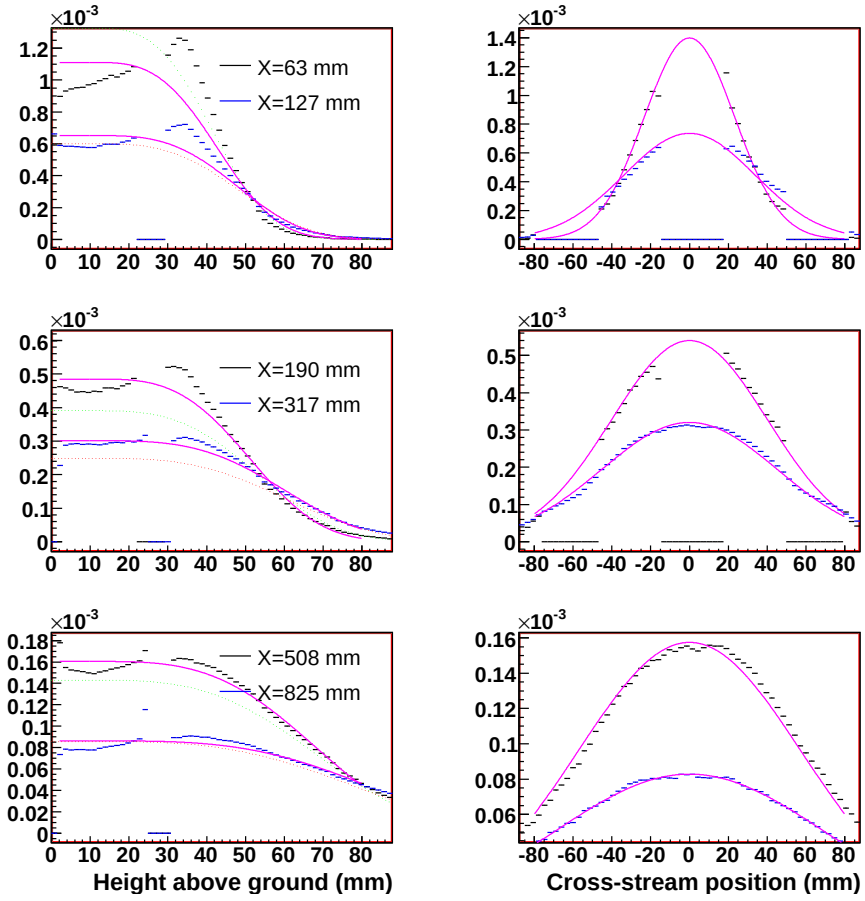

Figure 13: *Identical plots and array configuration as for Figure 12 except the source has been placed directly behind an object in the array. The functional form used in the fit is given by (53). Vertical axis is concentration and has been normalised by concentration of dye in the source pipe fluid and is dimensionless.*

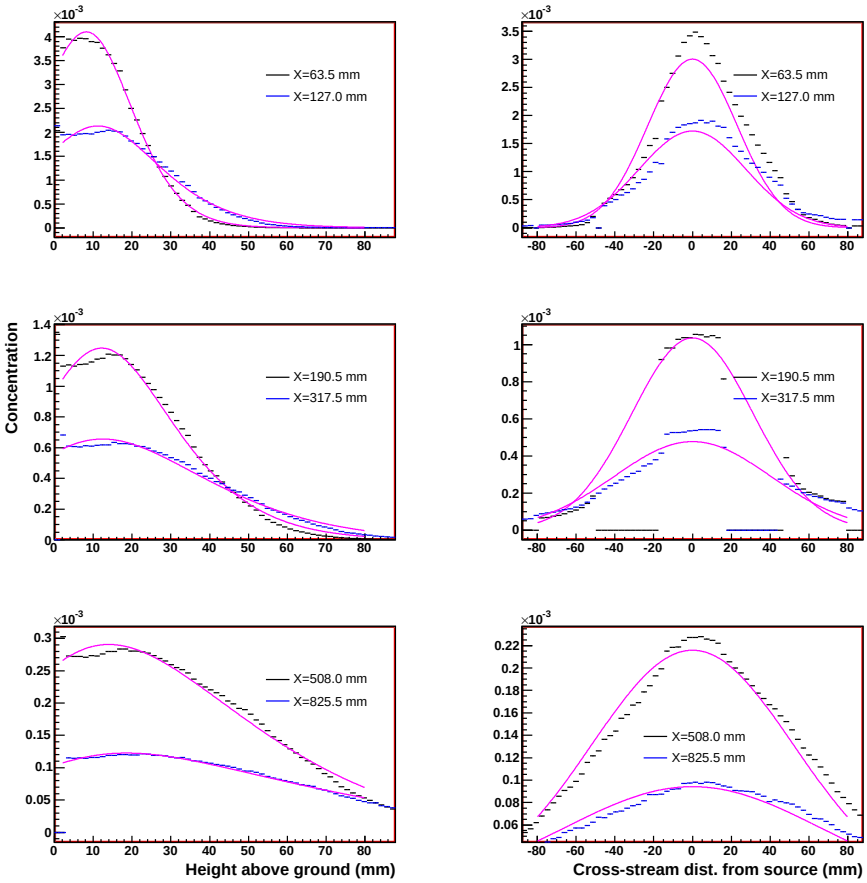

Figure 14: *Example of model fit for ground source in a canopy array. Vertical axis is concentration and has been normalised by concentration of dye in the source pipe fluid and is dimensionless. In each plot the magenta line shows the results of fitting (24) (vertical profiles) and a Gaussian function (horizontal profiles), but with α from (50). Better fit in the source region (top plot).*

The framework is also important as a first step in the development of models of concentration fluctuations in urban environments. Such models facilitate the generation of realistic plumes for synthetic environments used in operational analysis studies. Thus the strong internal variability and intermittency of the concentration field within a dispersing plume will be able to be captured. This will enable the calculation of realistic fluctuating CBR challenge levels, which will facilitate studies on optimal detection systems for CBR threats, provide the necessary input for models of toxicity response and data fusion algorithms for enhanced situational awareness, and is a cornerstone for the rigorous quantification of uncertainty in dispersion predictions.

Scope exists to refine the proposed modelling framework. This includes resolution of the un-physical behaviour of the displacement height d as the canopy drag parameter ϵ becomes very small. To provide a truly unified framework, a single functional form for the velocity framework would also be preferable. The problem here is that there is no analytical solution for the advection diffusion equation in a log-law boundary layer—the traditionally preferred description of a sheared flow boundary. With the stronger theoretical underpinning of the power law velocity profiles due to Barenblatt [5, 6], this could be a preferred option, however the flow model described in Section 3.1 would be ill-determined with the use of this functional form. There are options for a more complex specification of the profile with a variable power law exponent α that would enable a solution here, but this added complexity and extra parameterisation was not pursued in the first instance as reported here.

The equation (53) currently models what should happen to the tracer in the plume spreading over an urban canopy. However when comparing this model to experimental data, a model of how the equipment 'sees' a particular turbulent plume concentration is also needed, in order to accurately compare experiment and theory. This is because any experimental setup is not perfect. In the case of the Coanda experiment, a weakness lies in the equipment not being able to sense a concentration below a critical threshold, and as such part of the plume is not captured by the experiment,[19] resulting in apparent non-conservation of the plume in the data and deformation of the plume shape. Such a step is essential for the model to be able to predict not only what a plume would do, but how sensors and experiment would see the plume. It would also allow completion of the validation of the model with the Coanda data-set, such as in Figures 12 and 13.

This is suspected to be a key reason why a global fit of parameters for the model over the whole scope of a plume affected by an underlying canopy is poor. Other possible reasons are that the COANDA experiment's flow may be non homogeneous over the array (due to the array designers placing the plume sources near the beginnings of the arrays, instead of the middle) or that the model is missing some key behaviour. A combination of these causes is possible.

However, that the model can describe the plume well without an array, or with an array with individual fits for different downstream distances shows it captures much of the key physics.

The framework developed allows a link between previously published DSTO work on

[19]This problem is compounded by the rescaling of source concentrations and output data done for long upstream distance releases (done to improve detectability) combined with an unknown algorithm for cutting off noise which appears only partly dependent on the local average concentration.

fluctuating plume models in urban settings [30, 33], current DSTO–CSIRO collaborative work on internal concentration fluctuations [37], and more complex distributed drag CFD models in urban areas [18, 19, 20]. This will enable a high fidelity model of urban dispersion to be implemented for emergency response applications, with the extra capability for concentration fluctuation prediction and characterisation of the uncertainty in modelling predictions. Components of this technology may ultimately be transferred and integrated into a national Australian hazard prediction modelling system, should support be provided by civilian Government agencies.[20]

The framework developed has also provided a link through the UDM to another important operations analysis capability that DSTO now possesses—the CBR Virtual Battlespace developed by Dstl. There is further scope for development of concentration realisation models within this capability framework. Such models will rely more on simpler, faster approaches to dispersion modelling than CFD to enable rapid calculations for operational analysis tasks relying on exploration of high dimensional variable spaces, thus the framework developed here is ideal for these purposes.

Finally, the generation of prototype simple synthetic environments for plume realisations is also required to further develop data fusion algorithms for CBR source characterisation and network detection. The framework developed here is the first step in the development of such a synthetic environment at DSTO for these purposes, and can ultimately be used to compare the approaches studied at DSTO with those of our international collaborators.

[20] A project, funded by Emergency Management Australia, to undertake a scoping study for such a capability is currently underway .

References

1. Hall, D. J., A. M. Spanton, I. H. Griffiths, M. Hargrave, and S. Walker (2003): *The Urban Dispersion Model (UDM): Version 2.2*, Technical Documentation Release 1.1, Dstl/TR04774, 110 pp.

2. Lien, F. S., E. Yee, H. Ji, A. Keats, and K. J. Hsieh (2006): *Progress and chellenges in the development of physically-based numerical models for prediction of flow and contaminant dispersion in the urban environment*, International Journal of Computational Fluid Dynamics **20**, 323–337.

3. Yee, E., F. Lien, and H. Ji (2007): *Technical description of urban microscale modeling system: Component 1 of CRTI Project 02-0093RD*, DRDC-Suffield Technical Report, TR 2007-067, 46 pp.

4. Monin, A. S. and A. M. Yaglom (1971b): *Statistical Fluid Mechanics - vol 1, 2*, MIT Press, Cambridge Massachusetts.

5. Barenblatt, G. I., A. J. Chorin, and V. M. Prostokishin (2000): *Self-similar intermediate structures in turbulent boundary layers at large Reynolds numbers*, Journal of Fluid Mechanics **410**, 263–283.

6. Barenblatt, G. I. (2003): *Transfer of a passive additive in a turbulent boundary layer at very large Reynolds numbers*, Proceedings of National Academy of Sciences USA **100**, 1481–1483.

7. Gailis, R. M. (2005): *Wind tunnel simulations of the Mock Urban Setting Test—experimental procedures and data analysis*, DSTO–TR–1532, 47 pp.

8. Private communication from Dr. Eugene Yee, DRDC-Suffield, Canada.

9. Lettau, H. (1969): *Note on aerodynamic roughness-parameter estimation on the basis of roughness-element description.* Journal of Applied Meteorology **8**, 828–832.

10. Counihan, J. (1971): *Wind tunnel determination of the roughness length as a function of the fetch and the roughness density of three-dimensional roughness elements*, Atmospheric Environment **5**, 637–642.

11. Macdonald, R. W., R. F. Griffiths, and D. J. Hall (1998): *An improved method for the estimation of surface roughness of obstacle arrays*, Atmospheric Environment **32**, 1857–1864.

12. Macdonald, R. W., R. F. Griffiths, R. F., and D. J. Hall (1998): *A comparison of results from scaled field and wind tunnel modelling of dispersion in arrays of obstacles*, Atmospheric Environment **32**, 3845–3862.

13. Belcher, S.E., N. Jerram, and J. C. R. S. Hunt (2003): *Adjustment of a turbulent boundary layer to a canopy of roughness elements*, Journal of Fluid Mechanics **488**, 369–398.

14. Coceal, O., T. G. Thomas, I. P. Castro, and S. E. Belcher (2006): *Mean flow and turbulence statistics over groups of urban-like cubical obstacles*, Boundary-Layer Meteorology **121**, 491–519.

15. Coceal, O. and S. E. Belcher (2005): *Mean winds through an inhomogeneous urban canopy*, Boundary-Layer Meteorology **115**, 47–68.

16. Katul, G. G., L. Mahrt, D. Poggi, and C. Sanz (2004): *One- and two-equation models for canopy turbulence*, Boundary-Layer Meteorology **113**, 81–109.

17. Harman, I. N. and J. J. Finnigan (2007): *A simple unified theory for flow in the canopy and roughness sublayer*, Boundary-Layer Meteorology **123**, 339–363.

18. Lien, F. S., E. Yee, and J. D. Wilson (2005): *Numerical modelling of the turbulent flow developing within and over a 3-D building array, Part II: mathematical formulation for a distributed drag force approach*, Boundary-Layer Meteorology **114**, 245–285.

19. Lien, F. S. and E. Yee (2005): *Numerical modelling of the turbulent flow developing within and over a 3-D building array, Part III: a distributed drag force approach, its implementation and application*, Boundary-Layer Meteorology **114**, 287–313.

20. Lien, F. S., E. Yee, and Y. Cheng (2004): *Simulation of mean flow and turbulence over a 2D building array using high-resolution CFD and a distribued drag force approach*, Journal of Wind Engineering and Industrial Aerodynamics **92**, 117–158.

21. Cionco, R. M. (1965): *Mathematical model for air flow in a vegetative canopy*, Journal of Applied Meteorology **4**, 517–522.

22. Csanady, G. T. (1973): *Turbulent Diffusion in the Environment*, D. Reidel Publishing Company, Boston, MA, 248 pp.

23. Huang, C. H., (1979): *A theory of dispersion in turbulent shear flow*, Atmospheric Environment **13**, 423–443.

24. Nepf, H. M. (1999): *Drag, turbulence, and diffusion in flow through emergent vegetation*, Water Resources Research **35**, 479–489.

25. Mohan, M. and M. K. Tiwari (2004): *Study of momentum transfers within a vegetation canopy*, Pro. Indian Acad. Sci. (Earth Planet. Sci.) **113**, 67–72.

26. Raupach, M.R. and A. S. Thom (1981): *Turbulence in and above canopies*, Annual Reviews of Fluid Mechanics **13**, 97–129.

27. Massman, W. J. (1987): *A comparative study of some mathematical models of mean wind structure and aerodynamic drag of plant canopies*, Boundary-Layer Meteorology **40**, 179–197.

28. Yee, E., R. M. Gailis, A. Hill, T. Hilderman, and D. Kiel (2006): *Comparison of wind tunnel and water channel simulations of plume dispersion through a large array of obstacles with a scaled field experiment*, Boundary-Layer Meteorology **121**, 389–432.

29. Hilderman, T. and R. Chong (2005): *Requirement of high resolution, 2-dimensional tracer dispersion data for the development of atmospheric dispersion models within urban environment for air platforms*, DSTO Contract 130533, Coanda Research and Development Corporation report CRDC00391.

30. Skvortsov, A. T. and R. M. Gailis (2007): *Statistical Properties of a Meandering Plume in a Sheared Boundary Layer*, submitted to Boundary-Layer Meteorology.

31. Voulgaris, G. and J. H. Trowbridge (1998): *Evaluation of the acoustic doppler velocimeter (ADV) for turbulence measurements*, Journal of Atmospheric and Oceanic Technology **15**, 272–289.

32. `Root http://root.cern.ch/`

33. Gailis, R. M., A. Hill, E. Yee, and T. Hilderman (2006): *Extension of a fluctuating plume model of tracer dispersion to a sheared boundary layer and to a large array of obstacles*, Boundary-Layer Meteorology **122**, 577–607.

34. Davidson, M. J., K. R. Mylne, C. D. Jones, J. C. Phillips, R. J. Perkins, J. C. H. Fung, and J. C. R. Hunt (1995): *Plume Dispersion Through Large Groups of Obstacles—A Field Investigation*, Atmospheric Environment **29**, 3245–3256.

35. Wang, Y. and Cionco, R., 2007. *Wind Profiles in Gentle Terrains and Vegetative Canopies for a Three-Dimensional Wind Field (3DWF) Model*, Army Research Laboratory, ARL-TR-4178.

36. Davidson, M. J., W. H. Synder, R. E. Lawson Jr., and J. C. R. Hunt (1996): *Wind Tunnel Simulations of Plume Dispersion Through Groups of Obstacles*, Atmospheric Environment **30**, 3715–3731.

37. Borgas, M., Skvortsov, A. and Gailis, R. (2007): *Surface layer mixing properties: simple models for fluctuations*, manuscript under preparation.

38. Cowan, I. (1968): *Mass, heat, and momentum exchange between stands of plants and their atmospheric environment,* Quart. J. Roy. Meteor. Soc., **94**,523-544.

Appendix A New Plume Dispersion Model

A.1 Velocity Profile

The parameter σ, while not fundamental (it is totally determined by ϵ and γ) is important, because the formulae for U, K, d and z_0 cannot be written in terms of ϵ. Thus we have included a plot of its behaviour here (see Figure A1). The key features it has are that it decreases from a maximum in the sparse limit and approaches 0 at infinity. It is also very sensitive to γ, increasing sharply as γ increases.

Following on from this, it is worthwhile looking in more detail at what happens to the wind profile model in the extremes of very dense and very sparse canopies. For very dense canopies we get for $\epsilon \to \infty$

$$\begin{aligned}
d + z_0 &\to H, \\
d &\to H\left(1 - \frac{2(\gamma\kappa)^2}{\epsilon}\right) \to H, \\
z_0 &\to \frac{2H(\gamma\kappa)^2}{\epsilon e^1} \to 0, \\
\sigma &\to \frac{2(\gamma\kappa)^2}{\epsilon}, \\
U_- &\to \frac{u_*}{\gamma\kappa}\exp\left[\frac{\epsilon}{(\gamma\kappa)^2}\left(\frac{z}{2H} - \frac{1}{2}\right)\right] \to \begin{cases} 0 \text{ if } z < H \\ u_*/\kappa \text{ if } z = H \end{cases}, \\
K_- &\to \frac{\sigma H u_*}{\gamma\kappa}\exp\left[\frac{\epsilon}{2(\gamma\kappa)^2}\left(\frac{z}{H} - 1\right)\right] \to 0 \text{ for } z < H, \\
U_+ &\to \frac{u_*}{\gamma\kappa}\left[1 + \log\left(1 + \frac{(z-H)\epsilon}{2H(\gamma\kappa)^2}\right)\right] \to \begin{cases} \infty \text{ if } z < H \\ u_*/\kappa \text{ if } z = H \end{cases}, \\
K_+ &\to \gamma\kappa u_*(z - H).
\end{aligned} \tag{A1}$$

That $U_+(z) \to \infty$ in this limit shows that this theory does not well cover the case of an infinitely dense canopy. This is an artifact of the functional forms forcing the velocity to remain constant and non-zero at H, even as the effective ground height d rises to H. To negate this, it is necessary to let the velocity at the canopy top decrease to zero as ϵ increases to infinity, such that the velocity at the top of the ABL remains constant.

In the limit $\epsilon \to 0$ a different problem arises

$$\begin{aligned}
\sigma &\to 2(\gamma\kappa)^2, \\
d &\to -H, \\
z_0 &\to 2He^{-1}, \\
d + z_0 &\to 2(e^{-1} - 1)H, \\
V_- &\to \frac{u_*}{\gamma\kappa}\sqrt{\frac{z}{H}}, \\
K_- &\to 2\gamma\kappa u_*\sqrt{zH}, \\
V_+ &\to \frac{u_*}{\gamma\kappa}\left[1 + \log\left(\frac{z+H}{2H}\right)\right], \\
K_+ &\to \gamma\kappa u_*(z + H).
\end{aligned} \tag{A2}$$

The problem is that if $\epsilon = 0$ there should be no canopy, thus no behaviour change in $U(z)$ at $z = H$. For example this theory predicts a significant difference between wind passing over a perfectly flat field and a perfectly flat field with a few infinitesimally thin sticks standing upon it. The theory behaves sensibly in the $\epsilon \to 0$ limit only if the canopy height $H \to 0$ at the same time. However away from these extremes, the $U(z)$ and $K(z)$ profiles are very sensible and agree well with experiment (see Section 4.4). The lower limit of ϵ for which we can use this theory without concern is determined by when $d = 0$. The corresponding ϵ value is

$$\epsilon = 1.8336(\gamma\kappa)^2. \tag{A3}$$

A.2 Vertical concentration gradient within the canopy

This section provides a closer look at the predicted concentration within the canopy. Inserting the modelled formulae for $U(z)$ (41) and $K_{zz}(z)$ (38) into the advection-diffusion equation (21) yields

$$\frac{\partial C}{\partial x} = \frac{\sigma\beta}{2\tanh(\beta z/H)}\frac{\partial C}{\partial z} + H\sigma\frac{\partial^2 C}{\partial z^2}, \quad 0 < z < H. \tag{A4}$$

This is subject to the boundary condition that tracer material should not move below the ground:

$$\left.\frac{\partial C}{\partial z}\right|_{z=0}.$$

For typical values of the canopy parameter ϵ used in the Coanda experiment (designed to model an urban environment), $\tanh(\beta z/H)$ can be approximated by $\beta z/H$. This is especially true near the ground. The solution for (A4) can thus be approximated by

$$C_-(x, z) \propto x^{-3/4} \exp\left(-\frac{z^2}{4\sigma H x}\right), \quad 0 < z < H. \tag{A5}$$

The important observations to make here are that:
A) For $x > H/\sigma$ the exponent of e above would be small and thus C within the canopy would be close to constant a short distance downstream of the source,
B) The exponent α (50) should indeed be 2 at the ground.

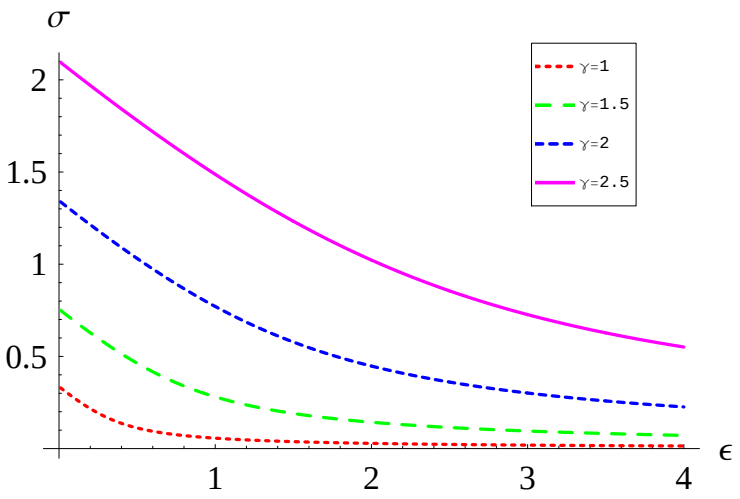

Figure A1: *The parameter σ against ϵ for various γ*

DEFENCE SCIENCE AND TECHNOLOGY ORGANISATION DOCUMENT CONTROL DATA	1. CAVEAT/PRIVACY MARKING

2. TITLE	3. SECURITY CLASSIFICATION
Turbulent Dispersion Modelling in a Complex Urban Environment – Data Analysis and Model Development	Document (U) Title (U) Abstract (U)
4. AUTHORS	5. CORPORATE AUTHOR
Alexei T. Skvortsov, Peter D. Dawson, Michael D. Roberts and Ralph M. Gailis	Defence Science and Technology Organisation 506 Lorimer St, Fishermans Bend, Victoria 3207, Australia

6a. DSTO NUMBER	6b. AR NUMBER	6c. TYPE OF REPORT	7. DOCUMENT DATE
DSTO–TR–2366	AR–014–674	Technical Report	February, 2010

8. FILE NUMBER	9. TASK NUMBER	10. SPONSOR	11. No. OF PAGES	12. No. OF REFS
2008-1116019-1	CDG 07/266	Project Director JP2110	37	38

13. URL OF ELECTRONIC VERSION	14. RELEASE AUTHORITY
http://www.dsto.defence.gov.au/corporate/reports/DSTO–TR–2366.pdf	Chief, Human Protection and Performance Division

15. SECONDARY RELEASE STATEMENT OF THIS DOCUMENT

Approved for Public Release

OVERSEAS ENQUIRIES OUTSIDE STATED LIMITATIONS SHOULD BE REFERRED THROUGH DOCUMENT EXCHANGE, PO BOX 1500, EDINBURGH, SOUTH AUSTRALIA 5111

16. DELIBERATE ANNOUNCEMENT

No Limitations

17. CITATION IN OTHER DOCUMENTS

No Limitations

18. DSTO RESEARCH LIBRARY THESAURUS

Plumes, Tracer dispersion, Turbulence, Modelling, Biological aerosols, Chemical defence, Radiological defence, Mathematics

19. ABSTRACT

This report summarises recent research conducted by the DSTO in plume model development for urban environments, with an emphasis on establishing clear physical grounds for the models, yet maintaining enough simplicity to be treated numerically in an operationally viable way. The aim is not to replace existing operational models with a new generation of more accurate models, but to provide a more physics-based framework for flow and dispersion in an urban environment that can reconcile the empirically based approach of current operational models, and the more sophisticated computational fluid dynamics techniques now gaining popularity for atmospheric dispersion applications. A key feature of the model framework developed in this report is the definition of a single parameter that describes canopy morphology, and links this to canopy flow variables. A simple canopy dispersion model is then developed, based on flow parameters generated by the canopy model. In relevant areas the well-known Urban Dispersion Model by the UK Defence Science and Technology Laboratory is used as a benchmark for comparison. Supporting evidence for the models developed here is supplied through comparison with experimental data from a water channel simulation.